WATER AND FLUORINE CONTENTS IN MT. HOOD MAGMAS RECORDED BY PLAGIOCLASE PHENOCRYSTS

A THESIS
SUBMITTED TO THE FACULTY OF THE
UNIVERSITY OF MINNESOTA
BY

JENNIFER RACHEL CASERES

IN PARTIAL FULFILLMENT OF THE REQUIREMENTS
FOR THE DEGREE OF
MASTER OF SCIENCE

MARC HIRSCHMANN

JULY 2019

Acknowledgements

I would first like to thank my advisor, Marc Hirschmann, for his support and guidance throughout my graduate school studies. Marc's door has always been open to me whenever I had a question or problem. I also thank Jed Mosenfelder, who taught me most of the lab techniques in this thesis and was there for the long SIMS trips. I am also grateful to Anette von der Handt for her instruction and assistance with electron microprobe analyses. I am also thankful for Yunbin Guan's assistance with SIMS analyses. I would also like to acknowledge my committee members, David Kohlstedt and Ikuko Wada. I am also grateful to Donna Whitney for providing feedback on this research by serving on my oral and written exam committees. Adam Kent and Alison Koleszar provided the plagioclase samples for this study. I really appreciate the insight into Mt. Hood and volcanology that Alison has shared with me.

I am also grateful for the incredible support system I've had during graduate school. The ESCI community is full of wonderful people, and I am thankful the friends I have made here. I cannot thank my family and friends enough for their continuous encouragement. My boyfriend, Nick, has been unfailingly supportive, and I am deeply grateful for him. Finally, the real MVPs are the cats who have had to put up with my procrastination harassment.

Dedication

I dedicate this thesis to my relentlessly supportive brother.

Abstract

Volatiles have a significant effect on the properties of minerals and melts, even when present in trace amounts. They impact the phase equilibria (Wyllie 1979; Gaetani and Grove 1998), rheological properties (Dingwell et al. 1985; Hirth and Kohlstedt 1996), and volcanic eruption dynamics (Roggensack et al. 1997; Cashman 2004). H_2O is the most well-studied volatile component of magmas, but other volatiles species (e.g. F) are the subject of increasing interest (Dasgupta and Dixon 2009). Magmatic volatiles are often measured in melt inclusions (MIs) (e.g. Straub and Layne 2003; Plank et al. 2013), but may be uncommon in some rocks or subject to post-entrapment modification (PEC) (Wallace 2005). Alternatively, measurements of volatiles in minerals can be used to calculate melt volatile contents with a known partition coefficient (e.g. Wade et al. 2008). In this study, concentration profiles of H_2O and F in plagioclase from Mt. Hood, OR are paired with previously studied MI volatile contents from the same pyroclasts (Koleszar et al. 2012) to assess the fidelity of H_2O and F records retained in volcanic plagioclase. The spatial resolution of secondary ion mass spectrometry (SIMS) analyses allows us to detect volatile loss, and possibly constrain syn- and post-eruptive processes.

Table of Contents

List of Tables

List of Figures

1. Introduction

1.1. Mt. Hood, Oregon

Mt. Hood is an andesitic arc volcano from the Cascadia subduction zone (Scott and Gardner 2017). Mt. Hood lava compositions and volatile contents overlaps those of explosive volcanoes in the Cascade, including Mt. St. Helens, the Three Sisters, and Crater Lake (Hildreth 2007), yet it has a consistently low explosivity (Koleszar et al. 2012). Studying Mt. Hood's different eruptive periods can shed light on the factors that influence eruption explosivity (Koleszar et al. 2012). There is a wealth of information available on its eruptive processes, including magma recharge (Kent et al. 2010; Cooper and Kent 2014), crystal residence time (Eppich et al. 2012), and eruption temperature (Koleszar et al. 2012). Crucial for extricating the effect of volatiles on these eruptions, Koleszar et al. (2012) analyzed MI volatile contents from Mt. Hood's three most recent eruptive periods. We will compare H_2O and F in plagioclase phenocrysts from the same eruptive units to assess plagioclase ability to record magmatic water and potentially syn-eruptive processes.

Mt. Hood's three most recent eruptive periods are in Old Maid (~200 years ago), Timberline (1.5 ka), and Polallie (15-30 ka) (Scott and Gardner 2017). Although the Old Maid eruptive period began in 1781 and lasted until the mid-1790s (Scott and Gardner 2017), logs from British naval Captain George Vancouver's 1792 expedition to the Pacific Northwest do not record any potential eruptive activity from Mt. Hood (Scott et al. 1997a). The expedition certainly saw Mt. Hood, as expedition member Lieutenant W.E. Broughton named the volcano for famous British naval officer A.A. Hood. However, the effects of Old Maid are not completely absent from the written record, as Lewis and Clark's

description of the Sandy River in 1805 suggest the river carried a sediment load significantly higher than today owing to volcaniclastic deposits from the Old Maid eruptions (Scott et al. 1997a).

Descriptions of volcanic activity are recorded in Native American legends of the brothers Wy'east and Pahto (Mts. Hood and Adams, respectively) battling over the beautiful Loowit (Mt. St. Helens). Wy'east and Pahto fought by hurling red-hot boulders at each other, until Tyee Sahale (commonly translated as "Great Spirit") separated them by collapsing the Bridge of the Gods between their territories. Wy'east is said to have won the favor of Loowit over Pahto, and Wy'east continued to burn while Pahto lay dormant. These legends correspond to geologic records, as Mt. Hood has been more active than Mt. Adams since the Last Glacial Maximum. The Bridge of the Gods was a land bridge formed in the Bonneville landslide, and may have collapsed in the 1700 Cascadia subduction zone earthquake (Harris 2005).

Mt. Hood continues to have mild fumarolic activity and sporadic earthquakes (Scott et al. 1997a), and is likely to erupt in the next few decades. A large explosive event with tephra fallout is not likely, but lahars would pose a threat to buildings, municipal water supplies, and roads (Scott et al. 1997b). Advance detection of potential eruptions would mitigate hazards and prevent loss of life. The insight into eruptive processes from volatile records in phenocrysts could be paired with other petrologic and geophysical observations to improve eruption forecasting.

1.2. Volatiles at the arc

1.2.1. Arc magma genesis and H_2O

H_2O is a key factor in the formation of arc volcanoes at subduction zones. Subducted oceanic crust carries volatiles into the mantle via hydrated minerals, sediments, and pore fluid (Faccenda 2014). Most subducted H_2O is derived from hydrated minerals in altered oceanic crust, as the oceanic crust forms the bulk of the subducted mass (Van Keken et al. 2011). Aqueous fluids are released from hydrated minerals through dehydration reactions (Schmidt and Poli 2013) (**Figure 2**). The nature of the H_2O-rich component sourced from the slab has been a source of debate. It may be a hydrous melt (Marschall and Schumacher 2012) or supercritical aqueous liquid (Kessel et al. 2005). Nevertheless, the H_2O-rich component travels upward through the mantle wedge to the base of the overlying lithosphere, where it produces melting to source arc volcanism (Grove et al. 2012).

The primary melts that form from the hydrous melting of the mantle wedge are basalts. Studies of MI from primitive arc basalts have H_2O contents that are roughly 4 wt%. This may reflect the water content of the magmas sourced from the mantle wedge, but may also be affected by a crustal control where measured H_2O content reflects vapor saturation at the depth of pre-eruptive storage (Plank et al. 2013). H_2O contents in some primitive magmas may be very high. Phase equilibria experiments on primitive magnesian andesites from Mt. Shasta indicate they were sourced from magmas with up to 14 wt% H_2O (Krawczynski et al. 2012).

Extracting the history of volatiles from evolved magmas is more complex. Silicic or intermediate magmas can be the product of closed system fractional crystallization

(Singer et al. 1992) or recharge of silicic crystal mushes with volatile-rich mafic magmas and subsequent magma mixing (Reubi and Blundy 2009). Study of the volatile history of these magmatic systems may answer questions regarding magma storage conditions, volatile inputs, and recharge history (Wright et al. 2012).

Andesites at Mt. Hood are the product of magma mixing between a dacitic to rhyolitic crystal mush stored in the crust and volatile-rich mafic recharge magma. The magma chamber may undergo multiple recharge events without erupting (Cooper and Kent 2014). If a recharge event results in eruption, it will occur ~2 weeks after recharge (Kent et al. 2010). Andesitic volcanoes are frequently explosive, but as a low-explosivity andesitic volcano, the volatile history of Mt. Hood can provide insight into the causes of explosive eruptions (Koleszar et al. 2012).

1.2.2. Explosivity and H_2O

Explosive eruptions pose a significant hazard to surrounding communities. Volatiles, particularly H_2O, exert control on eruption explosivity by changing melt viscosity and acting as propellants (Cashman 2004). Explosive eruptions occur when melt viscosity increases during H_2O exsolution and prevents bubble growth. Vapor continues to exsolve, and high bubble overpressure leads to brittle failure and fragmentation (Dingwell 1996; Forte and Castro 2019). The strong control of volatile contents on eruptive style is demonstrated by the 1992 and 1995 eruptions of Cerro Negro. The 1992 eruption was explosive, but the 1995 eruption was effusive. The eruptions had similar compositions, but magma storage depth was shallower in 1995 (1-2 km) than in 1992 (6 km). H_2O and CO_2

were degassed at shallower storage composition, and changed the eruptive style to effusive (Roggensack et al. 1997).

Temperature also influences eruptive style by altering viscosity. Higher magma temperatures may cause previously explosive volcanoes to erupt effusively (Ruprecht and Bachmann 2010). Lowered viscosity at higher temperatures allows bubbles to coalesce and relieves the overpressure and strain that leads to fragmentation, even at high volatile contents (Dingwell 1996; Cashman 2004). Mt. Hood contains similar volatile contents and a broadly similar composition as its more explosive neighbors, but the temperature increase post-magma recharge decreases its explosivity (Koleszar et al. 2012).

1.2.3. F in arc magmas

F also influences melt viscosity (Dingwell et al. 1985), but it is not commonly concentrated in primitive arc magmas (Webster et al. 2018). This is likely because F is not efficiently extracted from the subducted slab (Straub and Layne 2003). However, F is not readily degassed from the magma and acts as an incompatible element, so it can become highly concentrated during fractional crystallization (Balcone-Boissard et al. 2010). F is highly soluble in silicate melt, and can potentially be concentrated up to ~7 wt% (Dolejš and Zajacz 2018). Melts with high concentrations of F can exsolve fluids that deposit ore bodies (Dolejš and Zajacz 2018), and if F-rich melts erupt they can have a catastrophic effect on the ozone layer (Broadley et al. 2018).

1.3. Measuring volatiles

In order to evaluate the effects of volatiles on a magmatic system, they must be accurately measured in minerals and melts. There are a variety of methods to measure H_2O and F, and each method has its ideal application. Anorthite-albite exchange between plagioclase and melt can be used to calculate magmatic H_2O (Lange et al. 2009; Waters and Lange 2015), but it is not accurate when the system has been subjected to disequilibrium processes (Mollo et al. 2011). Melt inclusions and nominally anhydrous minerals more accurately record volatile contents immediately prior to eruption.

1.3.1. Melt inclusions

Melt inclusions (MIs) are a direct sample of magma trapped within a growing crystal. Volatile contents of MIs can be measured, although care must be taken to ensure that they are representative of the original contents of the melt. Melt inclusion contents can be modified by post entrapment crystallization (PEC), diffusive loss and re-equilibration, or leakage. Incompatible elements will be enriched in the remaining melt during PEC while the walls of the melt inclusion crystallize, so the amount of crystallized material must be added back to the MI to calculate the initial chemistry. Chemical species that diffuse quickly through the host crystal, such as hydrogen through olivine (Ingrin and Blanchard 2006), may re-equilibrate or be lost when conditions surrounding the crystal change (Plank et al. 2013). Loss may also happen via leakage along cleavage planes in the host crystal. Analysis of MIs is a powerful tool to measure volatile contents, but additional methods can provide a complementary dataset or be applied where there is a dearth of MIs.

1.3.2. Nominally anhydrous minerals

Nominally anhydrous minerals (NAMs) are minerals that do not contain H in their ideal chemical formula, but are often found to incorporate trace amounts of H (Bell and Rossman 1992). Trace amounts of H are typically incorporated in NAMs in the form of OH groups, but may also be present as H_2O (Johnson and Rossman 2004) or H_2 (Yang et al. 2016). Although speciation of H in minerals and melts may not necessarily be H_2O, we will broadly refer to incorporated H as H_2O for simplicity.

NAMs can be used to determine initial H_2O content with a known partition coefficient between melt and the mineral of interest. The partition coefficient describes the distribution of a chemical species between two phases, and is defined as

$$D_{H_2O}^{mineral-melt} = \frac{C_{H_2O}^{mineral}}{C_{H_2O}^{melt}} \quad (1)$$

where $D_{H_2O}^{mineral-melt}$ is the partition coefficient H_2O between minerals and melts, $C_{H_2O}^{phase}$ is the concentration of H_2O in a particular phase. The partition coefficient can be determined by experimental equilibration of a mineral and melt (e.g. Tenner et al. 2009; Hamada et al. 2013) or by measurement of MIs and the surrounding crystal (e.g. Johnson 2005; Seaman et al. 2006).

NAMs must be rapidly cooled to preserve their pre-eruptive volatile contents, but this method has proven effective for small volcanic pyroclasts. Clinopyroxene has been used to measure magmatic H_2O from arc volcanoes with a range of H_2O contents (Wade et al. 2008). Concentration profiles in clinopyroxene, along with the diffusion coefficient of H, have also been used to constrain ascent rate (Lloyd et al. 2016).

Volatiles in plagioclase feldspar

Plagioclase feldspar, $(Ca,Na)[Al(Al,Si)Si_2O_8]$, is a NAM abundant in intermediate magmas and thus would be a useful recorder of magmatic volatiles. Additionally, H is incorporated into plagioclase only as OH groups (Johnson and Rossman 2003). Changes in speciation may produce a non-Henrian relationship between mineral and melt H_2O concentrations and complicate application of a NAM hygrometer. Speciation is more complex in alkali feldspars: H_2O can be found in anorthoclase and microcline, and NH_4^+ is found in hyalophane and microcline (Johnson and Rossman 2004).

Plagioclase is expected to retain H_2O to an equal or greater extent as other NAMs. Plagioclase H diffusion (Johnson and Rossman 2012) is comparable to proton-vacancy controlled H diffusion (Demouchy and Mackwell 2006) in olivine, and slower than redox-controlled (Kohlstedt and Mackwell 1998). Plagioclase H_2O loss is also expected to be comparable to (Hercule and Ingrin 1999) or slower than (Woods et al. 2000) H_2O loss from natural diopside at temperatures relevant to andesitic arc volcanoes. The retention of H_2O in plagioclase is further supported by high H_2O concentrations, up to 1950 µg/g, found in some volcanic feldspars (Johnson and Rossman 2004, with FTIR absorption coefficient corrected after Mosenfelder et al. 2015).

Previous studies of $D_{H_2O}^{plag-melt}$ are summarized in **Table 1**. Changes in conditions such as pressure, temperature, oxygen fugacity, melt and mineral composition may affect the partitioning behavior (Yang 2012). Thus, it is important to select a $D_{H_2O}^{plag-melt}$ that has been determined at conditions similar to the desired application. The $D_{H_2O}^{plag-melt}$ measured

from plagioclase and MI from Mt. St. Helens (Johnson 2005), a dacitic arc volcano also in the Cascades, is the most relevant of the previously determined partition coefficients.

1.3.3. Measurement techniques

Accurate calculation of magmatic volatiles from NAM volatile contents requires diligent analysis because H is often difficult to quantitatively measure, especially in trace amounts. It is not directly measurable by electron microprobe, and methods such as weight loss upon heating or x-ray structure refinement are only reliable for H_2O contents of several tenths of a weight percent or higher (Rossman 2006). Fourier-transform infrared (FTIR) spectroscopy can directly measure lower amounts of H_2O using Beer's law,

$$A = \epsilon l c \tag{2}$$

where A is the peak absorbance of the IR band, ϵ is a molar absorption coefficient, l is the path length through the sample, and c is the concentration of the species of interest in the sample. The absorption coefficient must be determined by some external method such as manometry (Aines and Rossman 1984), extraction and continuous flow mass spectrometry (O'Leary et al. 2007), electron recoil detection analysis (Sweeney et al. 1997) or nuclear magnetic resonance (NMR) spectroscopy (Johnson and Rossman 2003). Of the aforementioned techniques, FTIR has become the most widely used because the instrument is relatively accessible and affordable (Rossman 2006).

Secondary ion mass spectrometry (SIMS) has proven to be a powerful method for analyzing volatile elements (Hauri et al. 2002; Koga et al. 2003; Mosenfelder et al. 2011, 2015; Mosenfelder and Rossman 2013), and it is increasing in popularity as standards are

calibrated (Rossman 2006). SIMS can be used in conjunction with FTIR (e.g. Koleszar et al. 2012) where only a subset of samples are not suitable for FTIR or information about speciation is desirable. Additionally, SIMS offers better spatial resolution than FTIR. Quantitative transects are easily attainable in anisotropic minerals, whereas analysis of twinned or cracked crystals is difficult with FTIR (Johnson and Rossman 2003). Core-rim transects of volcanic plagioclase are useful for assessing the extent of volatile loss in a phenocryst. This is a key advantage over FTIR for this application, as FTIR would integrate through regions with volatile loss and underestimate concentrations. With a significant diffusion profile, FTIR would underestimate the amount of H_2O for a given thickness of plagioclase.

Fluorine

Another advantage of SIMS is the ability to analyze multiple elements simultaneously. F is easily ionized for SIMS and typically has a very low detection limit of < 1 µg/g (Hauri et al. 2002). It is expected to be more compatible in nominally halogen-free minerals than Cl (Dalou et al. 2012), and could provide insight into halogen systematics in arc volcanoes. F concentrations in plagioclase are typically < 5 µg/g but may be as high as 39 µg/g (Mosenfelder et al. 2015). F loss from minerals is likely slower than H loss, based on orthopyroxene dehydration/defluorination (Mosenfelder and Rossman 2013), so it may retain magmatic F even over prolonged cooling times.

2. H_2O and F records in Mt. Hood plagioclase phenocrysts

2.1. Background

Nominally anhydrous minerals (NAMs) incorporate trace amounts of H_2O and F (Bell and Rossman 1992; Mosenfelder and Rossman 2013; Mosenfelder et al. 2015). The volatile contents of the most recently equilibrated magma can be calculated with a known partition coefficient between the mineral and melt. Clinopyroxene has been shown to record magmatic water, and ascent rate can be calculated from H_2O concentration profiles of rapidly cooled pyroxene (Wade et al. 2008; Lloyd et al. 2016). Volcanic plagioclase can retain high H_2O contents (Johnson and Rossman 2004), and diffusive loss of H_2O from plagioclase (Johnson and Rossman 2012) is expected to be comparable to (Hercule and Ingrin 1999) or slower than (Woods et al. 2000) H_2O loss from clinopyroxene. We expect that plagioclase can retain magmatic H_2O if rapidly cooled, as it would be in pyroclasts that are cm-scale or smaller. In this study, we pair SIMS analyses of H_2O and F in plagioclase with melt inclusion (MI) data (Koleszar et al. 2012) from the same Mt. Hood pumice pyroclasts. We will test the ability of plagioclase to record magmatic H_2O and F, and consider the potential of plagioclase to record syn- or post-eruptive processes.

2.2. Methods

2.2.1. Samples and preparation

Feldspar-rich separates from single pumice pyroclasts in Old Maid (pyroclast MH08-20), Timberline (MH08-22), and Polallie (MH08-23) eruptive units were provided by the authors of Koleszar et al. (2012). Pumice pyroclasts were roughly ~10 cm (A. Koleszar, personal communication, March 12, 2019). Single plagioclase phenocrysts without pervasive cracks or mineral inclusions were selected for analysis. Phenocrysts

were prepared using established epoxy-free methods (Hauri et al. 2002; Koga et al. 2003; Aubaud et al. 2007; Mosenfelder et al. 2011) to lower the H background during SIMS analysis. Phenocrysts were mounted on bullet stubs with cyanoacrylate glue, ground to ~50% of their original height, and polished to 0.3 μm using diamond lapping film and diamond polishing powder. Some phenocrysts were imaged in the electron microprobe before SIMS analysis, and carbon coat was subsequently removed with 1 μm diamond lapping film. Phenocrysts were removed from bullet stubs with acetone, then cleaned in three 15-minute baths of acetone and three 15-minute baths of isopropanol in a sonicator before mounting in indium. Indium mounts were pressed flat with a laboratory press, then baked at 50°C overnight in a vacuum oven. The mounts were sputter coated with 20-60 nm gold and then inserted into the 7f-GEO airlock.

2.2.2. Electron microprobe

Major element analyses on plagioclase phenocrysts and inclusions from the 2016 session were performed using a JEOL JXA8900R at the University of Minnesota. Beam conditions of 15 kV and 20 nA were used for WDS, with a defocused beam of 10 μm to prevent the devolatilization of Na during WDS analysis. Counting times for all elements were 10 seconds. Natural oxides and silicates were used for standards: albite (Si, Na), ilmenite (Ti, Fe), anorthite (Ca, Al), forsterite (Mg), orthoclase (K), Mn-rich olivine (Mn), and chromite (Cr). Core to rim transects of phenocrysts were performed to confirm the agreement of our analyses with Koleszar et al. (2012).

Imaging of phenocryst major element zoning was performed using JEOL JXA8900R and a JEOL JXA-8530F Plus Hyperprobe at University of Minnesota. Beam

conditions of 15 kV and 60 nA were used for imaging. EDS analyses on plagioclase phenocrysts and inclusions from the 2018 session were conducted with JEOL JXA-8530F Plus Hyperprobe using beam conditions of 15 kV and 20 nA.

2.2.3. Secondary ion mass spectrometry

H and F analyses were performed by secondary ion mass spectrometry using a CAMECA IMS 7f-GEO ion microprobe at Caltech over two sessions. Analytical procedures for both sessions are similar. We followed previously described procedures to lower the H background (Hauri et al. 2002; Koga et al. 2003; Aubaud et al. 2007; Mosenfelder et al. 2011). The instrument was baked for 24 hours after inserting the mounts into the sample exchange airlock, and the samples were held in the sample exchange airlock for an additional 36 hours prior to analysis. A liquid N_2 cold trap was used to lower the H background in session 1, but not in session 2.

A Cs^+ ion beam with a current of 4-5 nA was used to sputter the sample with an accelerating voltage of 9 kV. Analysis spots were pre-sputtered for 2 minutes with a 15 μm raster, and a 100 μm field aperture was used to collect ions from the central 3 μm of the crater. 20 cycles of ^{12}C, $^{16}O^{1}H$, ^{18}O, ^{19}F, ^{30}Si were collected. ^{35}Cl was collected during some analyses to identify mixed analyses with melt inclusions. ^{12}C was used to assess hydrocarbon contamination.

Plagioclase standards for H_2O (Mosenfelder et al. 2015) and synthetic basalt glass standards for F (Guggino and Hervig 2011) and measured ratios $^{16}O^{1}H/^{18}O$ and $^{19}F/^{18}O$ from the standards were used to construct H_2O and F calibration lines. A York fit (York 1966), implemented with R package IsoplotR (Vermeesch 2018), was used to calculate the

standard line from plagioclase H standards. There are no matrix-matched standards for plagioclase for F, so we used silicate glass standards that were used in previous studies of F in NAMs, including feldspar (Mosenfelder and Rossman 2013; Mosenfelder et al. 2015). Parameters for fits are included in **Appendix C.**

Three to five points were acquired on most phenocrysts to estimate variation throughout the crystal. Larger phenocrysts (>300 μm in one direction) were typically analyzed in the center and at four cardinal points around the edge. Three spots were taken along the long dimension of smaller phenocrysts. Additional analyses were collected on selected phenocrysts to further assess variation across the crystal.

2.3. Results

2.3.1. Major element and texture

The plagioclase composition range of the measured phenocrysts is An_{36} to An_{67} (**Appendix D**), which is similar to the composition range reported by Koleszar et al. (2012). Koleszar et al. (2012) also reported rhyolitic (71 to 77 wt% SiO_2) MI in all eruptive units. Plagioclase phenocrysts from each eruptive unit have distinct size ranges and a variety of major element and volatile zoning patterns (BSE images and SIMS maps in **Appendix A**).

Polallie phenocrysts are equant to prismatic with short dimensions as small as 0.2 mm and long dimensions up to 0.9 mm. The Polallie phenocrysts have simple oscillatory zoning with some resorption features (**Figure 3c**), and fewer melt inclusions than plagioclase from other eruptive units examined here. Polallie phenocrysts analyzed in this study are An_{42} to An_{52}, which is narrower than the range of An_{39} to An_{64} observed in Koleszar et al. (2012).

Timberline phenocrysts are ~0.5 to 1.5 mm in size and have a variety of major element zoning patterns, from homogenous (**Figure 3b, 4a**) to oscillatory zoning with complex zoning and resorption features. The compositions are similar to those reported by Koleszar et al. (2012), and cores of the Timberline phenocrysts are consistently more anorthitic than the rims. Small 1-10 μm MIs are present in bands associated with resorption features (**Figure 4b, 4c**). These MIs are too small to measure quantitatively with WDS but mixed analyses show they are more Si rich than the surrounding plagioclase (**Appendix D**). This enrichment in Si could reflect post-entrapment crystallization (PEC), or it may reflect the dacitic to rhyolitic MI compositions typical of other MI in this sample (Koleszar et al. 2012).

Old Maid phenocrysts are the largest, from ~1 to 1.5 mm. They also have oscillatory zoning with compositions from An_{36} to An_{66} with resorption features. Old Maid phenocrysts have inclusions of ilmenite, apatite, and orthopyroxene, as well as MIs (**Appendix D**). MIs appear in bands of small (~5 μm) inclusions, as in the Timberline phenocrysts, and as larger rounded or elongated inclusions up to 50 μm. Larger MI often have significant PEC and exsolved gas bubbles.

2.3.2. H_2O zoning

Phenocrysts from the Polallie pyroclast have the highest H_2O concentrations, from 67 to 110 μg/g H_2O, with maxima from 87 to 110 μg/g H_2O. Timberline phenocrysts have a wide range of H_2O concentrations, from 42 to 102 μg/g H_2O, and maxima in each phenocryst ranges from 52 to 102 μg/g H_2O. Old Maid has lower concentrations than the other two eruptive units. H_2O concentrations range from below the detection limit to 44

μg/g H_2O, with maxima in each phenocryst varying from 9 to 44 μg/g H_2O. Maxima and minima for each phenocryst are presented in **Table 2**, and maxima for each phenocryst are plotted against the mean length in **Figure 5a**.

The lowest H_2O concentrations tend to be on the crystal rims, and the highest in the center (**Figure 3**). Core to rim transects for selected phenocrysts typically have a gradual, constant slope from maximum to lower edge concentrations, but one plagioclase from Timberline showed a flat top with a steep drop off in concentration (**Figure 3**). Apparent reverse H_2O zoning is noted in one phenocryst from Timberline (**Figure 4b**).

2.3.3. F zoning

F concentrations and maxima in the plagioclase for each eruptive unit vary less between eruptive units than H_2O zoning, although there are some notable differences in zoning between units. Plagioclase from each eruptive unit had F concentrations from ~ 2 to 4 μg/g F (**Table 2**), with two outliers: one Timberline phenocryst had anomalously high 7.9 μg/g F, and one Old Maid phenocryst had F below the detection limit. Maxima for each phenocryst are plotted against mean phenocryst length in **Figure 5b**.

Similar to H_2O zoning, F zoning is typically normal zoning, with lower F concentrations on phenocryst rims and higher concentrations in the center. (**Figure 3, Appendix A**). Core to rim transects for selected phenocrysts typically have flatter shape and drop off gradually towards the edge. However, there is there is an inverse correlation between H_2O and F in Timberline phenocrysts (**Figure 6a**) that is not present in Polallie and Old Maid phenocrysts. This correlation can be observed as reverse F zoning with normal H_2O zoning in an individual phenocryst (**Figure 6b**).

2.4. Discussion

2.4.1. Construction of a hygrometer

Constructing a hygrometer from analyses of H_2O in plagioclase requires consideration of processes that might modify the H_2O content post-equilibration, such as degassing. It also relies on accurate measurements of MI H_2O contents in equilibrium with the measured plagioclase. The resulting $D_{H_2O}^{plag-melt}$ may be compared to previous studies of the partition coefficient to check for agreement. Provided that these conditions are met, the measured H_2O in plagioclase can be converted to H_2O melt concentrations independent of another hygrometer.

Constraints on maximal values in plagioclase phenocrysts

Magmatic H_2O in plagioclase can be modified by syn-eruptive degassing during ascent, and through volatile loss during post-eruptive cooling. The potential effects of these processes can be minimized by selecting rapidly-cooled rocks from explosive eruptions (Lloyd et al. 2013, 2016). The ~10 cm pumice pyroclasts examined here would cool slower than ash or lapilli, but it is possible that phenocrysts retain pre-eruptive H_2O contents in their core. Olivine-hosted MI from similarly pumice bombs have been found to have a range of H_2O contents from extensively degassed to minimal loss (Lloyd et al. 2013). Plagioclase H diffusion (Johnson and Rossman 2012) is comparable to proton-vacancy controlled H diffusion (Demouchy and Mackwell 2006) in olivine, and slower than redox-controlled (Kohlstedt and Mackwell 1998). Thus, plagioclase phenocrysts from ~10 cm pumice pyroclasts can also be expected to retain a range of H_2O contents, with some values approaching the pre-eruptive H_2O content. Analyses of multiple phenocrysts and

consideration of core-rim transects as potential H_2O diffusive loss will allow assessment of the extent of volatile loss.

Polallie phenocrysts have the narrowest range of H_2O contents, and maxima are clustered together with a mean value of 93 ± 3 μg/g H_2O. H_2O contents do not typically vary more than ~10 μg/g throughout the phenocryst (**Table 2**). Consistent H_2O contents within and between phenocrysts indicates plagioclase H_2O is not substantially modified from pre-eruptive concentrations. The Polallie pyroclast in this study must have been erupted and cooled rapidly enough to quench plagioclase with minimal diffusive loss.

Timberline phenocrysts show more variation between maximum H_2O contents in each phenocryst. H_2O loss profiles in most phenocrysts have a sinusoidal shape, consistent with H diffusion out of the crystal. One phenocryst, MH08-22-11, shows a plateau that is interpreted to be very close to equilibrium (**Figure 3b**). The H_2O concentration falls off sharply at the edge. The maximum value of 102 μg/g H_2O, which is also the maximum value in all Timberline phenocrysts, is likely very close to the pre-eruptive value. MH08-22-11 is also the largest Timberline phenocryst in this study and may retain high its H_2O because diffusive loss did not reach the core over the timescale of cooling.

Old Maid phenocrysts have less H_2O than phenocrysts from Polallie and Timberline, although MI H_2O contents are similar (Koleszar et al. 2012). Old Maid phenocrysts have also lost a larger percentage of H_2O than phenocryst from Timberline and Polallie pyroclasts. This H_2O loss may have occurred during prolonged cooling. The significant PEC in MI from Old Maid phenocrysts is also consistent with slower cooling.

Extensive H_2O loss from Old Maid phenocrysts highlights the importance of geologic context when measuring magmatic H_2O in plagioclase. The Old Maid pyroclast

was resting on top of a block and ash flow and was rounded in a way consistent with entrainment in the block and ash flow, while Polallie and Timberline pyroclasts were not rounded (A. Koleszar, personal communication, March 12, 2019). The Old Maid eruptive period was also less explosive than the Timberline and Polallie eruptions. Old Maid was mainly a dome-forming eruption, with limited tephra distribution (Scott and Gardner 2017). Ascent rates for the Old Maid eruptive period would be slower than the more explosive Polallie and Timberline eruptions (Cashman 2004; Rutherford 2009).

Melt inclusions

This study does not include MI analyses, but instead utilizes the MI dataset for Mt. Hood presented by Koleszar et al. (2012). The plagioclase phenocrysts used in this study are from the same pyroclasts as the MIs measured by Koleszar et al. (2012). The highest MI volatile contents for each pyroclast are interpreted as the least affected by degassing. The MI with the highest H_2O in each sample are not plagioclase-hosted, but rather in orthopyroxene and amphibole (**Table 3**). Plagioclase-hosted MI contain lower H_2O contents but are likely affected by degassing post-equilibration or leakage along cleavage planes. H_2O contents calculated by anorthite-albite exchange (Koleszar et al. 2012, calculated with Lange et al. 2009) are higher and similar to concentrations recorded in the most hydrous orthopyroxene- and amphibole-hosted MI (Koleszar et al. 2012).

Partition coefficient

Maximum H_2O contents in plagioclase phenocrysts and in MI from Koleszar et al. (2012) and the resulting $D_{H_2O}^{plag-melt}$ are listed in **Table 3**. The partition coefficients for the Polallie and Timberline pyroclasts are comparable to Johnson (2005), with revised values

after Mosenfelder et al. (2015) (**Figure 7**). The partition coefficient for the Old Maid pyroclast is lower, owing to significant loss of H_2O in plagioclase while MI H_2O contents are similar to the other eruptive units.

Comparison to other studies of partition coefficient

The agreement of $D_{H_2O}^{plag-melt}$ with Johnson (2005) is expected because Mt. Hood is an arc andesite with dacitic MI and Mt. St. Helens is an arc dacite. Major differences in melt or feldspar composition may change the solubility of H_2O in one phase, and therefore affect $D_{H_2O}^{plag-melt}$. Other studies of $D_{H_2O}^{plag-melt}$ have focused on MORB and arc basalt (Hamada et al. 2013). Hamada et al. (2013) reported a variation in $D_{H_2O}^{plag-melt}$ between H_2O poor (≤1 wt%) and H_2O rich (≥4 wt%). The H_2O-rich partition coefficient is appropriate for our samples, and our measurement of $D_{H_2O}^{plag-melt}$ is very similar to the value of $D_{H_2O}^{plag-melt} = 0.003 \pm 0.001$. Variation of $D_{H_2O}^{plag-melt}$ between basaltic and dacitic melt does not appear to be significant, although further experimental study of $D_{H_2O}^{plag-melt}$ with andesitic and dacitic melt is needed.

This study provides additional insight into application of a $D_{H_2O}^{plag-melt}$ hygrometer through SIMS analyses, which allows greater spatial resolution. Considering the variation within a phenocryst enables us to search for a maximum value. FTIR integrates through the crystal and may underestimate if there is a significant diffusion profile.

Application of a hygrometer based on $D_{H_2O}^{plag-melt}$

This hygrometer is particularly useful where there is MI are not common. It could also be used in conjunction with MI H_2O measurements and other hygrometers. Anorthite-

albite exchange hygrometers (e.g. Lange et al. 2009; Waters and Lange 2015) have significant error with any disequilibrium (Mollo et al. 2011), but may be used to provide another constraint on pre-eruptive H_2O (e.g. Koleszar et al. 2012; Wright et al. 2012). This method is ideally applied to rapidly quenched rocks, such as pumices from fallout deposits. It is still possible to constrain a maximum value in the plagioclase for less rapidly-cooled samples, as seen in the Timberline plagioclase, but it requires core-rim transects and analyses of multiple crystals. Prolonged cooling might erase pre-eruptive H_2O, as in the case of Old Maid plagioclase. A SIMS study of the diffusivity of H in plagioclase would augment current diffusion data based on FTIR (Johnson and Rossman 2012) and provide further constraints on the timescale of post-equilibration modification.

Although careful selection of rapidly-cooled pyroclasts can mitigate potential diffusive loss, the results of a $D_{H_2O}^{plag-melt}$ hygrometer should nevertheless be interpreted as a constraint on the minimum H_2O in the magma. It is impossible to ensure that the true maximum in a pyroclast is measured. In theory, the highest H_2O is retained in the center of the phenocryst, but it is unlikely to sample the true center of a phenocryst. The phenocryst may have been broken during eruption or sample preparation, as the major element zonation shows in **Figure 2**. They may also not be ground to the exact middle of the phenocryst and analysis may sample an area with more diffusive loss than the true core.

2.4.2. Fluorine

F concentrations in feldspar have less variation between phenocrysts than H_2O (**Figure 3, 5**). Highest F concentrations are typically in the center of Old Maid and Polallie

phenocrysts. Even in Old Maid plagioclase with extensive H_2O loss, F concentrations remain similar to values in Timberline and Polallie phenocrysts. Old Maid phenocrysts show an F degassing trend with size, similar to that seen for H_2O in Timberline (**Figure 5**). F diffusion must be significantly slower than H_2O, as all Old Maid phenocrysts lost H_2O, but larger phenocrysts retained F. This has been observed in another NAM, as defluorination was observed to be slower than dehydration in orthopyroxene (Mosenfelder and Rossman 2013).

Unlike Old Maid and Polallie phenocrysts, Timberline phenocrysts have an inverse correlation between F and H_2O (**Figure 6**). Increased F at phenocryst rims likely represents interaction with an F-rich melt where incompatible F is enriched through fractional crystallization. The anti-correlation with H_2O might indicate that this F-rich melt contains less H_2O than the melt in equilibrium with the phenocryst core. Interaction with this melt could be occurring at a shallower depth where H_2O solubility in the melt is decreased. These trends might also be decoupled, with F gain occurring without significant H_2O loss. H_2O could then be lost during ascent and eruption. Gained F would then be minimally affected owing to slower diffusive loss.

F contents of MI from Mt. Hood are ~ 500 μg/g (Koleszar et al. 2012). Maxima from each eruptive unit are ~ 4 μg/g F, so the partition coefficient can be estimated as $D_F^{plag-melt} \cong 0.008$. This is on the low end of previous measurements of $D_F^{mineral-melt}$ for NAMs (Joachim et al. 2015; Rosenthal et al. 2015), but F is expected to be less compatible in plagioclase than olivine, orthopyroxene, clinopyroxene and garnet (Dalou et al. 2012). The retentivity of F in plagioclase, even after prolonged cooling, indicates that it

is potentially a powerful method to measure magmatic F. This method would become robust with further measurements of F in natural plagioclase/MI pairs and experimental studies of $D_F^{plag-melt}$.

2.4.3. Volatile records

Magma chamber equilibration

Andesitic arc volcanoes have complex histories, particularly with respect to volatiles. Hot, volatile-rich recharge magmas mix with cooler silicic crystalline mushes (Reubi and Blundy 2009) and may trigger eruption. If the recharged magma chamber does not erupt, it will cool to ~750°C. These magma chambers spend a majority of the time in this cold storage (Cooper and Kent 2014). If eruption is triggered, there is a ~2 week latency period between recharge and eruption (Kent et al. 2010). We must consider the equilibration time of H_2O between plagioclase and magma to determine if phenocryst H_2O concentrations reflect pre- or post-recharge magmatic H_2O. The time required for H diffusion into a phenocryst can be approximated as

$$t \cong \frac{x^2}{6D} \tag{3}$$

where t is time, x is distance to the phenocryst center, and D is the diffusion coefficient. The temperature after magma mixing and prior to eruption was ~950°C at Mt. Hood, obtained from oxide geothermometry (Koleszar et al. 2012). The diffusion coefficient for H in plagioclase is 10^{-13} m^2 s^{-1} at 950°C (Johnson and Rossman 2012). Phenocrysts vary from 0.2 to 1.5 mm, so equilibration would occur in ~5 to 11 days. All phenocrysts would equilibrate in the ~2 week period between recharge and eruption (Kent et al. 2010), so phenocryst H_2O contents were established post-recharge.

Syn- and post-eruptive processes

Maximal H_2O contents in plagioclase and MI indicate that it must have equilibrated at ~7 km, at vapor saturation of 5 wt% (Wallace and Anderson 2000; Plank et al. 2013), or deeper if the melt is undersaturated in H_2O. This is consistent with crystallization pressures of 100-200 MPa (4-8 km) for the plagioclase population crystallized in the magma chamber (Cooper and Kent 2014).

Post-equilibrium volatile modification may occur syn-eruption within the conduit, or post-eruption during cooling. The effect of post-eruptive cooling can be minimized by selecting small pyroclasts, which are likely to be rapidly-cooled as discussed earlier and by Lloyd et al. (2013). The timescale of post-eruptive cooling is difficult to constrain for plagioclase phenocrysts in this study, as they may have been cooled at different rates within the pyroclast.

Syn-eruptive volatile loss is determined by magma ascent rate. As magma ascends in the conduit during an eruption, the solubility of H_2O in the melt decreases and H_2O in the magma can decrease. Retention of H_2O in equilibrium with magma chamber H_2O requires rapid eruption to avoid re-equilibrating with shallower, drier melts. **Equation 3** can also be used to approximate the time needed to modify the core of a phenocryst during an eruption. Timberline phenocryst MH08-22-11 is ~1 mm and retains magmatic H_2O at its core, so ascent must have been faster than ~5 days to retain magmatic H_2O. Polallie phenocryst MH08-23d also retains magmatic H_2O and is ~0.5 mm, so ascent time for the Polallie eruption must have been faster than ~1 day. The ascent rate from ~7 km depth would be at least 0.02 m/s and 0.1 m/s for the Timberline and Polallie eruptions, respectively. The Timberline ascent rate is typical of dome-forming eruptions and the

Polallie ascent rate is approaching a Strombolian eruption (Cashman 2004; Rutherford 2009; Lloyd et al. 2016). Tephra distribution is widest for the Polallie eruption (Scott and Gardner 2017), which indicates it was potentially more explosive (Cashman 2004). A more sophisticated model to constrain ascent rate with H_2O concentration profiles in pyroxene (Lloyd et al. 2016) may be modified to constrain the ascent rates in the Polallie and Timberline eruptions with phenocryst data here. These models do not take into account post-eruptive loss upon cooling, so must be treated as minimal constraints on the ascent rate.

5. Conclusion

We have demonstrated that plagioclase phenocrysts from pumice pyroclasts may be used to measure magmatic H_2O and F. As a hygrometer, this technique would be most simple when applied to rapidly cooled phenocrysts from lapilli. Phenocrysts from larger, and therefore more slowly cooled (Lloyd et al. 2013), pyroclasts still retain magmatic H_2O but may require a greater number of both phenocrysts analyzed and analyses on each phenocryst to acquire an accurate maximum. F is likely better retained in plagioclase, and even slowly cooled samples could possibly retain high F. Volatile concentration profiles may also be combined with diffusion data to constrain a lower bound on volcanic ascent rate.

3. Future work

3.1. Partitioning studies

Further study of both $D_{H_2O}^{plag-melt}$ and $D_F^{plag-melt}$ would make measurement of magmatic H_2O and F in plagioclase more rigorous. Johnson's (2005) study of $D_{H_2O}^{plag-melt}$ uses natural plagioclase-MI pairs and could be augmented by an experimental dataset. The degree of control available for experimental studies of partitioning provides confidence that the partition coefficient is established at equilibrium. The combination of experimental and MI data from Hamada et al. (2013) show non-Henrian behavior of $D_{H_2O}^{plag-melt}$, which merits further investigation. This effect is attributed to a speciation change in the plagioclase, although OH is the only species in plagioclase determined by FTIR studies (Johnson and Rossman 2003). This non-Henrian behavior would be unusual behavior for a NAM, as this trend is not observed in olivine and orthopyroxene (Aubaud et al. 2004; Hirschmann et al. 2009). This result merits further investigation to ensure that an appropriate $D_{H_2O}^{plag-melt}$ is applied for all potential H_2O concentrations in the melt.

There are currently no studies focused on the partitioning of F between plagioclase and melt. $D_F^{plag-melt}$has been indirectly studied through determination of F partitioning between lherzolite-melt (Dalou et al. 2012). A preliminary $D_F^{plag-melt} \leq 0.02$ has been reported by Caseres et al. (2017), but these experiments were performed on conditions relevant to lunar anorthosites are likely not appropriate for arc andesites. There is clearly a need for more studies of $D_F^{plag-melt}$.

3.2. Diffusion studies

There is currently one study of H diffusion out of plagioclase (Johnson and Rossman 2012), and no studies of F diffusion for plagioclase. H loss from plagioclase was previously measured with FTIR (Johnson and Rossman 2012), and further study of H diffusion in plagioclase with SIMS would enrich the current dataset with increased spatial resolution. Johnson and Rossman (2012) found no anisotropy for H diffusion out of plagioclase, although this contrasts to other anisotropic minerals such as olivine (Kohlstedt and Mackwell 1998; Demouchy and Mackwell 2006). SIMS analyses on oriented plagioclase could either reveal anisotropy or more rigorously show that diffusion is isotropic. A well constrained diffusion coefficient of H for plagioclase would improve the accuracy of ascent rates constrained with H_2O profiles in plagioclase.

There are no studies of F diffusion for plagioclase or other nominally fluorine-free minerals. The F gain observed in the Timberline phenocrysts indicates that plagioclase may retain information about systematics of F during arc volcanism. Although it is currently difficult to ascertain where or when this increase in magmatic F occurred, diffusion studies could place additional constraints on the timing of F gain.

Tables

Study	$D_H^{fsp/melt}$	$D_H^{fsp/melt}*$	Feldspar composition	Melt composition	Data type
Johnson 2005	0.004	0.002	Labradorite	Dacitic	MI
Seaman et al. 2006	0.1	0.05	Anorthoclase	Phonolitic	MI
Hamada et al. 2013	0.01** 0.005***	0.005 0.003	Bytownite	Basaltic	MI and experiment

Table 1. *Previous studies of the partition coefficient of hydrogen between feldspar and melt. *Recalculation based on the revised FTIR absorption coefficient (Mosenfelder et al. 2015). **Water-poor conditions, H_2O in melt ≤ 1 wt%. ***Water-rich conditions, H_2O in melt ≥ 4 wt%.*

Eruptive unit	Phenocryst	Max H_2O (µg/g)	Min H_2O (µg/g)	Max F (µg/g)	Min F (µg/g)
Polallie	MH08-23-02	91(5)	87(5)	3.7(3)	3.5(2)
Polallie	MH08-23-05	92(4)	90(3)	4.1(4)	3.3(2)
Polallie	MH08-23-06	97(4)	66(3)	3.5(3)	2.2(3)
Polallie	MH08-23-13	95(4)	80(4)	3.5(3)	3.2(3)
Polallie	MH08-23-14	87(3)	75(4)	3.0(2)	2.6(2)
Polallie	MH08-23-15	97(3)	83(3)	3.4(4)	3.3(2)
Polallie	MH08-23-16	92(4)	87(3)	3.5(2)	3.2(2)
Polallie	MH08-23-17	90(4)	84(4)	4.2(4)	3.6(3)
Polallie	MH08-23a	105(6)	101(5)	3.1(3)	3.1(4)
Polallie	MH08-23b	107(7)	95(4)	3.2(4)	3.1(3)
Polallie	MH08-23c	101(7)	89(6)	3.4(4)	3.2(4)
Polallie	MH08-23d	110(9)	102(6)	3.2(3)	3.1(3)
Timberline	MH08-22-02	72(4)	41(3)	3.9(2)	2.7(2)
Timberline	MH08-22-06	69(3)	45(6)	3.9(3)	2.5(2)
Timberline	MH08-22-08	93(3)	52(3)	3.4(3)	2.0(3)
Timberline	MH08-22-11	102(5)	77(3)	2.5(3)	2.1(2)
Timberline	MH08-22-15	79(4)	42(6)	4.6(3)	2.3(2)
Timberline	MH08-22-18	60(3)	46(3)	4.2(3)	3.2(3)
Timberline	MH08-22-24	55(3)	45(8)	3.8(3)	3.3(3)
Timberline	MH08-22-28	85(4)	70(3)	2.6(3)	2.3(3)
Timberline	MH08-22-29	55(4)	46(2)	4.0(2)	3.3(3)
Timberline	MH08-22-32	51(2)	50(7)	3.8(3)	3.3(3)
Timberline	MH08-22-33	66(3)	47(2)	7.9(8)	2.5(3)
Timberline	MH08-22-36	72(4)	48(3)	3.6(3)	2.5(3)

Eruptive unit	Phenocryst	Max H_2O (µg/g)	Min H_2O (µg/g)	Max F (µg/g)	Min F (µg/g)
Timberline	MH08-22a	93(5)	60(7)	2.7(3)	2.2(3)
Timberline	MH08-22b	77(6)	73(4)	2.5(4)	2.4(4)
Timberline	MH08-22c	90(4)	50(3)	3.7(3)	2.0(4)
Timberline	MH08-22d	101(5)	86(6)	2.4(5)	1.9(3)
Old Maid	MH08-20-03*	8(1)	6(1)	2.4(3)	1.5(1)
Old Maid	MH08-20-04	42(4)	b.d.l.**	3.6(3)	b.d.l.
Old Maid	MH08-20-09	15(2)	2(1)	4.3(5)	1.6(2)
Old Maid	MH08-20a	28(3)	13(2)	1.7(2)	1.3(2)
Old Maid	MH08-20c	44(3)	15(1)	1.5(3)	1.2(2)
Old Maid	MH08-20d	16(3)	6(1)	2.7(3)	1.3(2)

Table 2. *Summarized results from each phenocryst. Complete data and maps shown in Appendix. *MH08-20-03 analyses do not cover a significant area. **b.d.l. signifies below detection limit. Errors are 2σ.*

Eruptive unit	Maximum H_2O (µg/g) in plagioclase	Maximum H_2O (wt%) in MI	MI host mineral	$D_{H_2O}^{plag-melt}$
Polallie	110(9)	5.1(2)	Orthopyroxene	0.0022(2)
Timberline	102(4)	5.4(2)	Amphibole	0.0019(1)
Old Maid	42(4)	5.4(2)	Orthopyroxene	0.0008(1)

Table 3. *Calculated partition coefficients from plagioclase maxima from each pyroclast sample, and corresponding MI maxima (Koleszar et al. 2012). Errors are 2σ.*

Figures

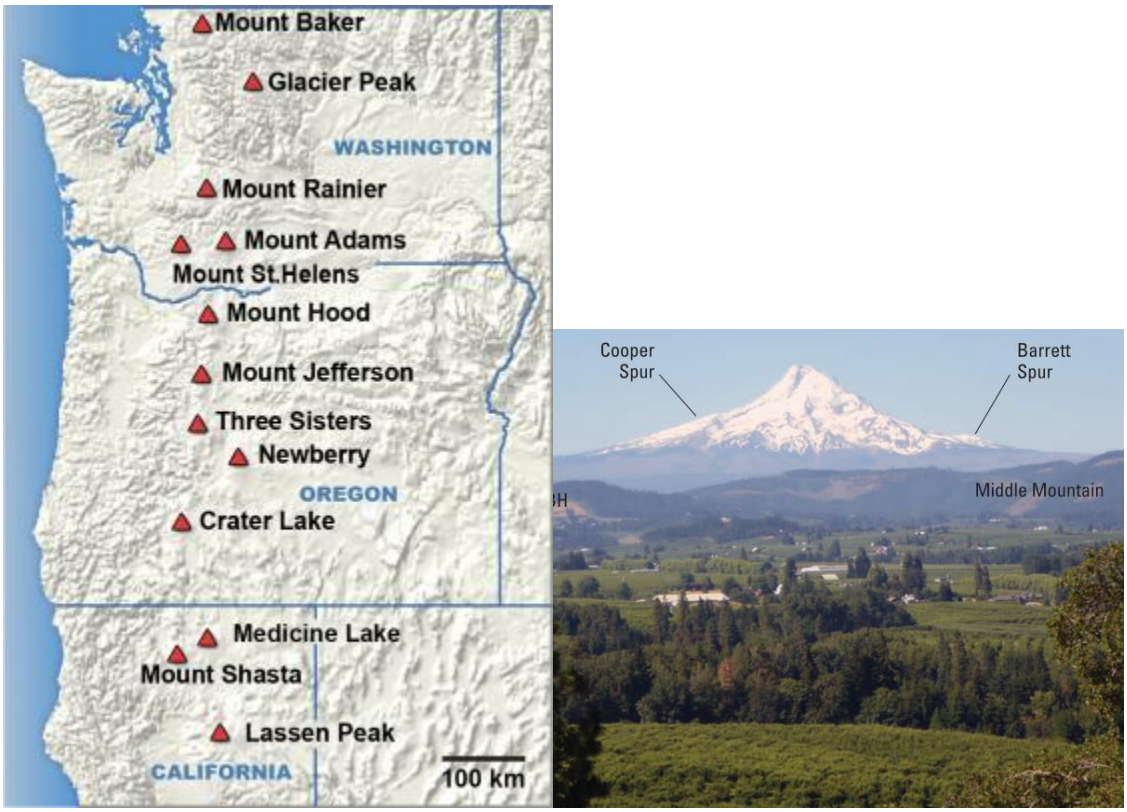

Figure 1. *Left, Map of Mt. Hood and other Cascades volcanoes (USGS CVO), and image of the volcanic edifice* (Scott and Gardner 2017).

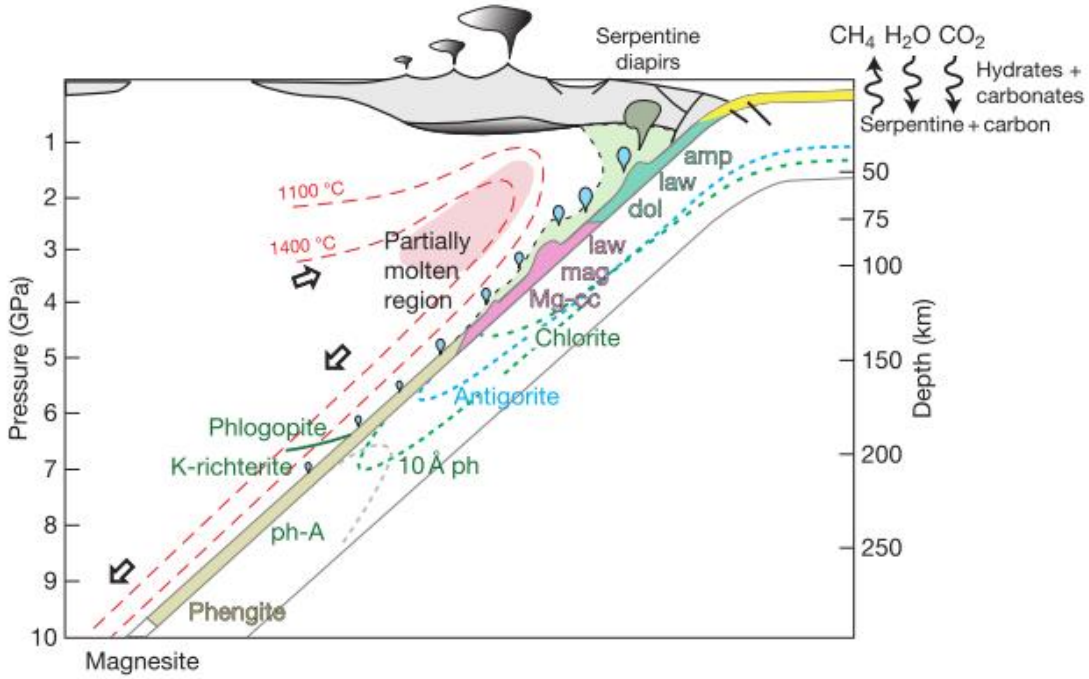

Figure 2. *Devolatilization reactions in the subducting slab* (Schmidt and Poli 2013).

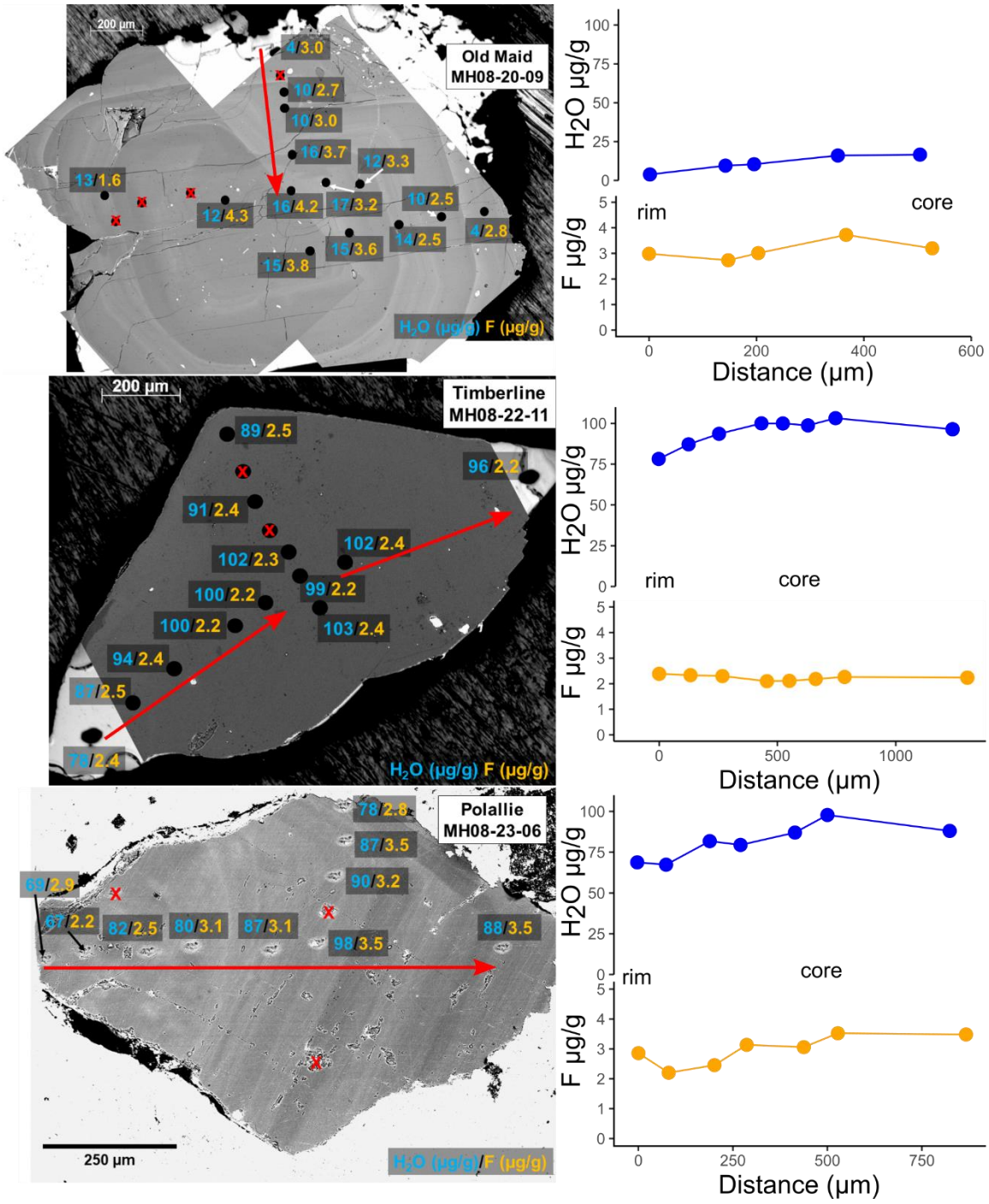

Figure 3. *BSE images of selected phenocrysts from each eruptive unit (left) and rim to core transects of these phenocrysts (right).*

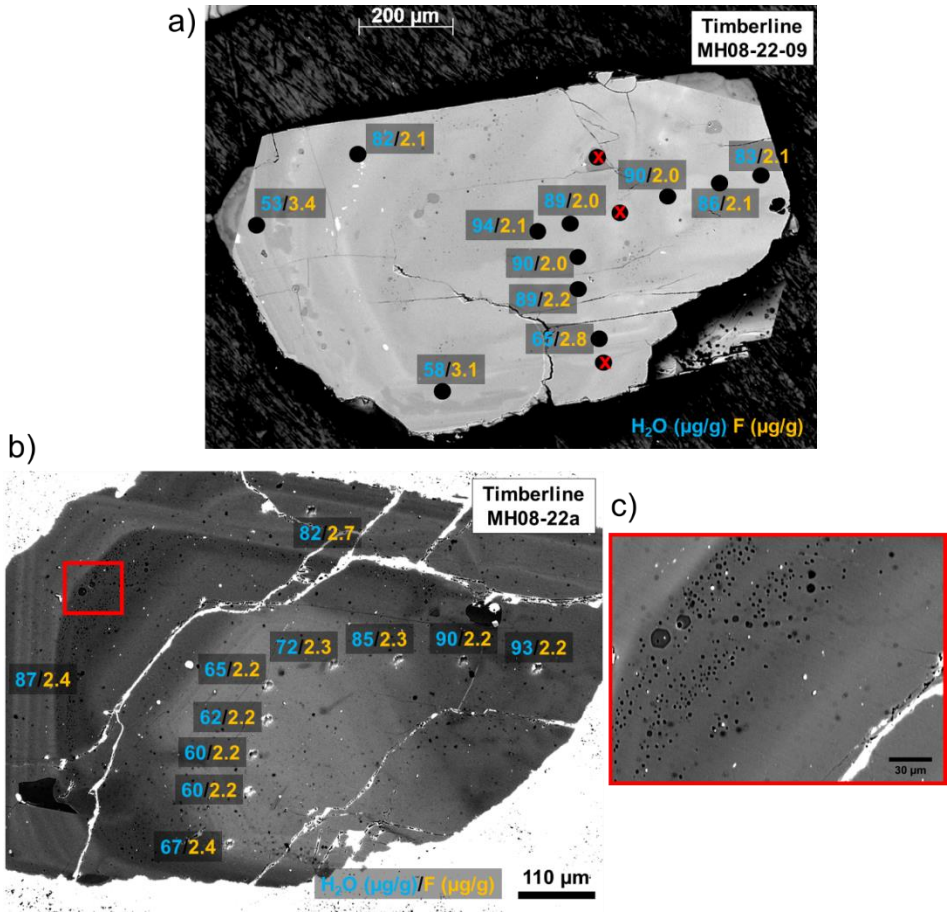

Figure 4. *Additional BSE images and H_2O/F maps: a) Timberline phenocryst with significantly different major element zoning than Figure 1b, but similar H_2O concentrations. b) Apparent reverse zonation of H_2O c) Band of small MI*

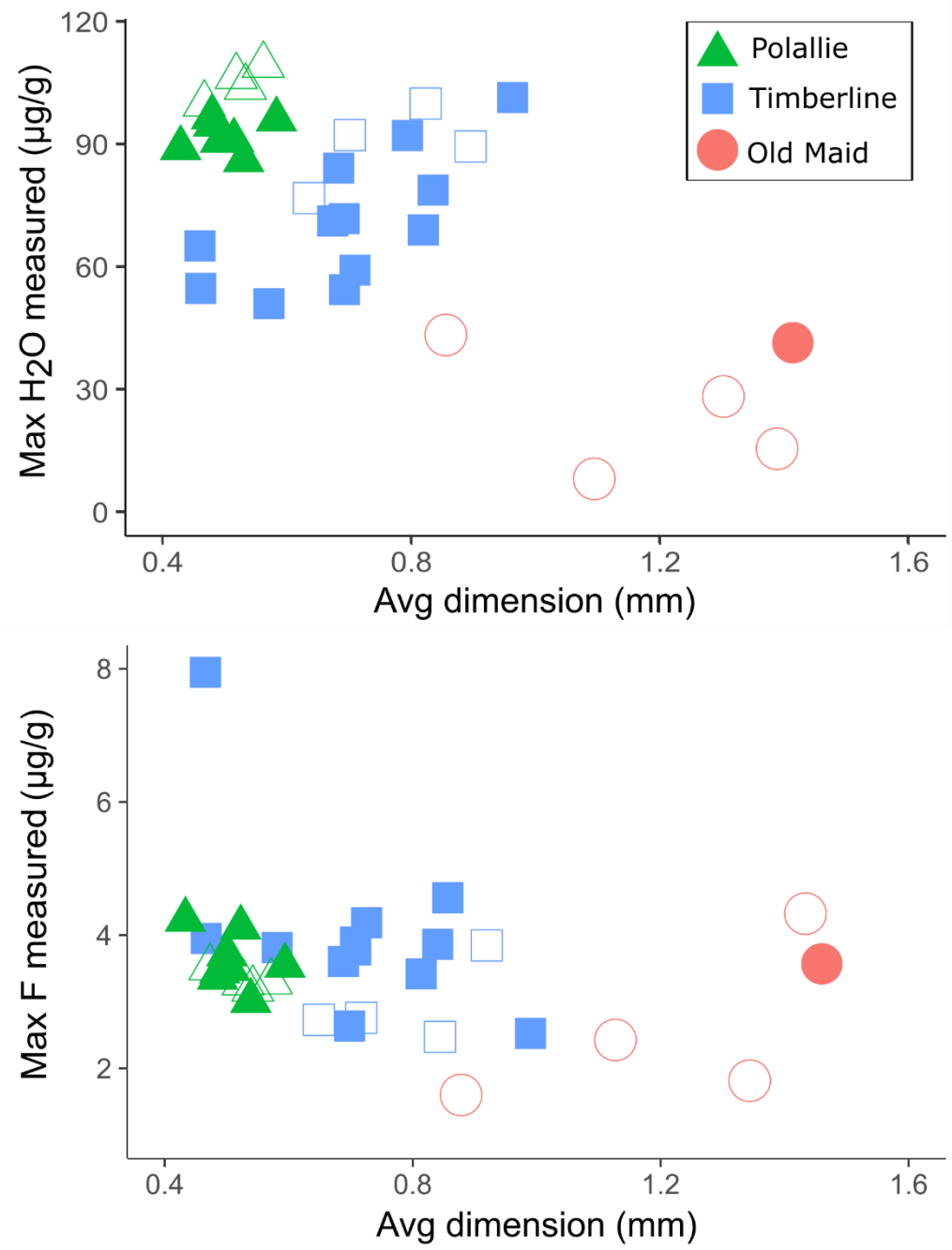

Figure 5. *H_2O and F concentrations plotted against phenocryst size, represented by the mean of three directions measured. Phenocrysts that have only two directions measured and are represented by open symbols.*

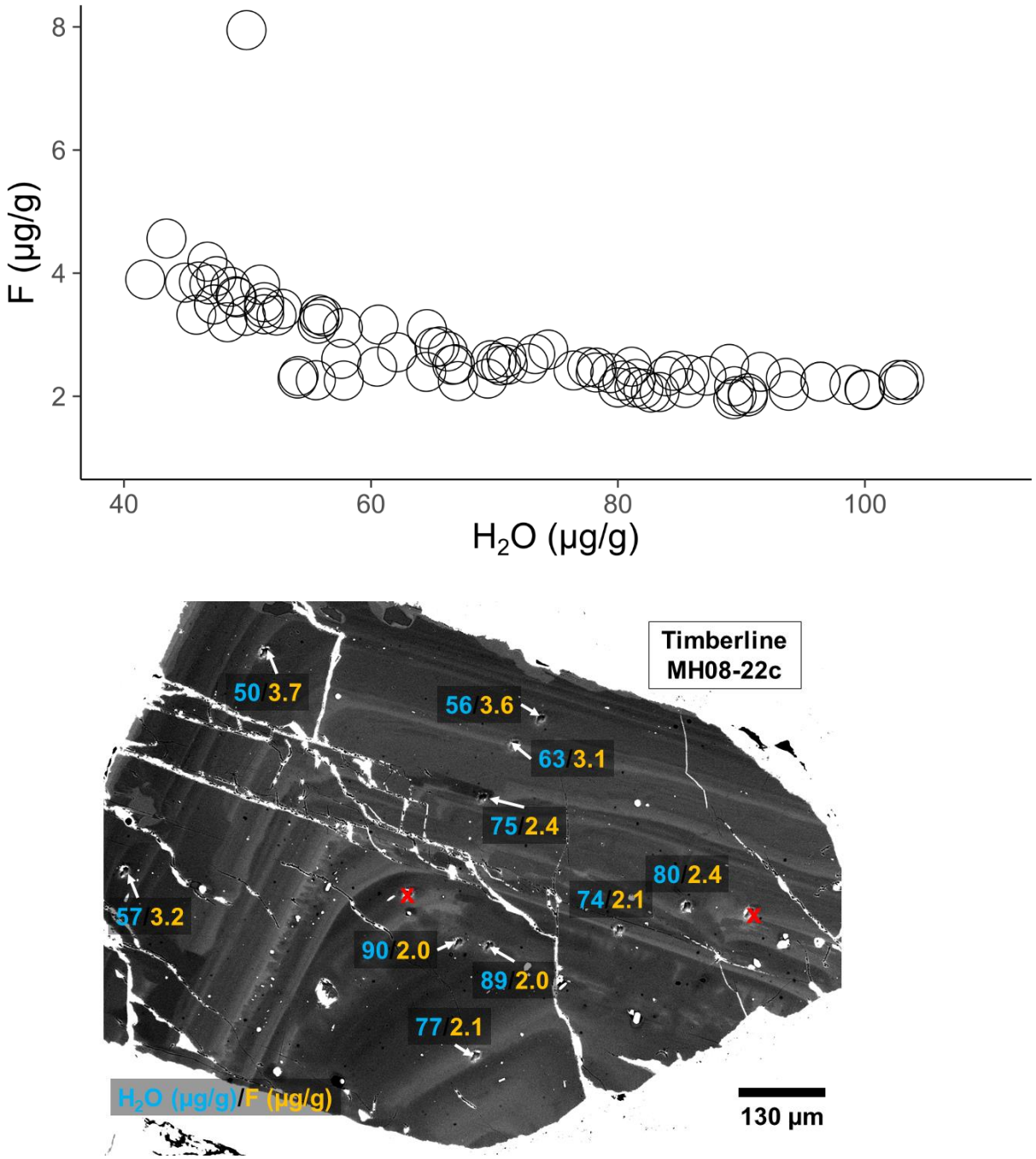

Figure 6*. Anti-correlation between F and H_2O in Timberline plagioclase, all analyses on Timberline phenocrysts (top), and anti-correlation in map (bottom).*

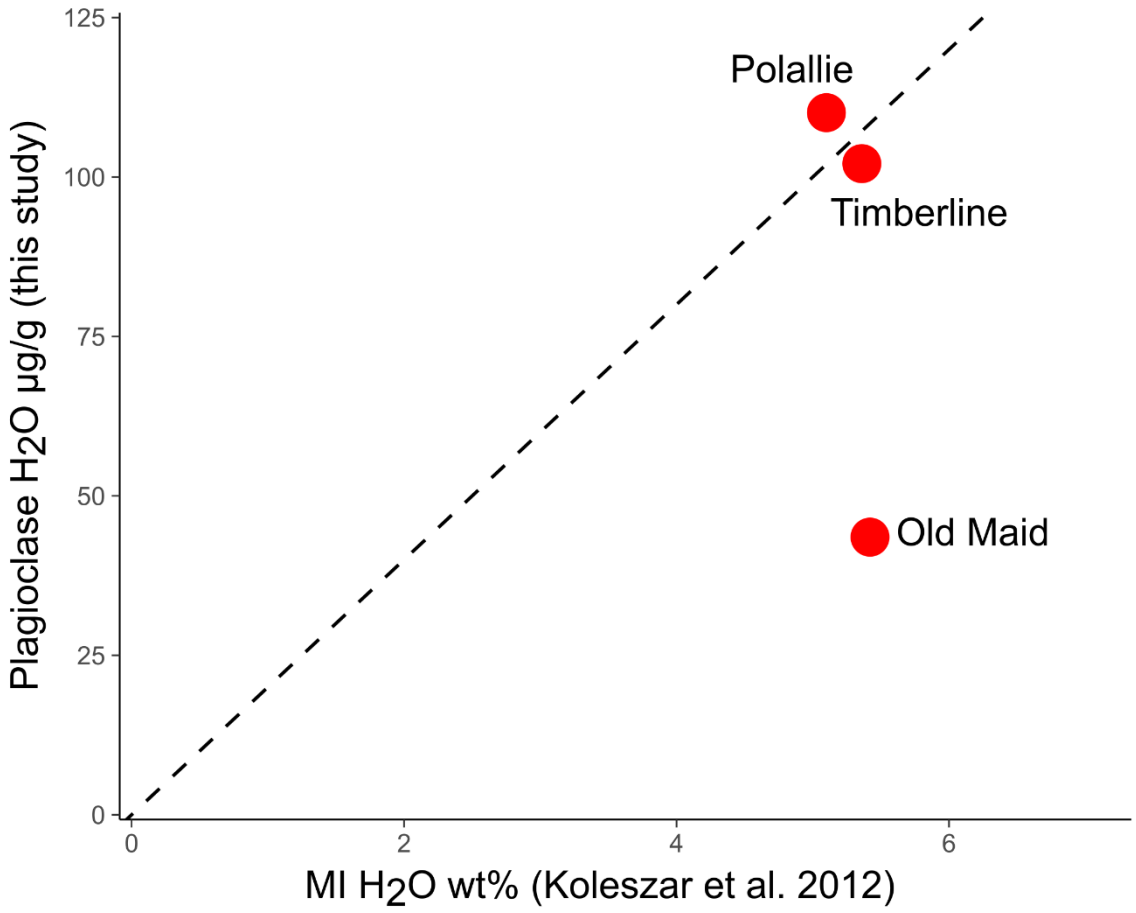

Figure 7. *$D_{H_2O}^{plag-melt}$ calculated for the three eruptive units (**Table 3**). Dotted line represents $D_{H_2O}^{plag-melt} = 0.002$ (Johnson 2005, revised after Mosenfelder et al. 2015).*

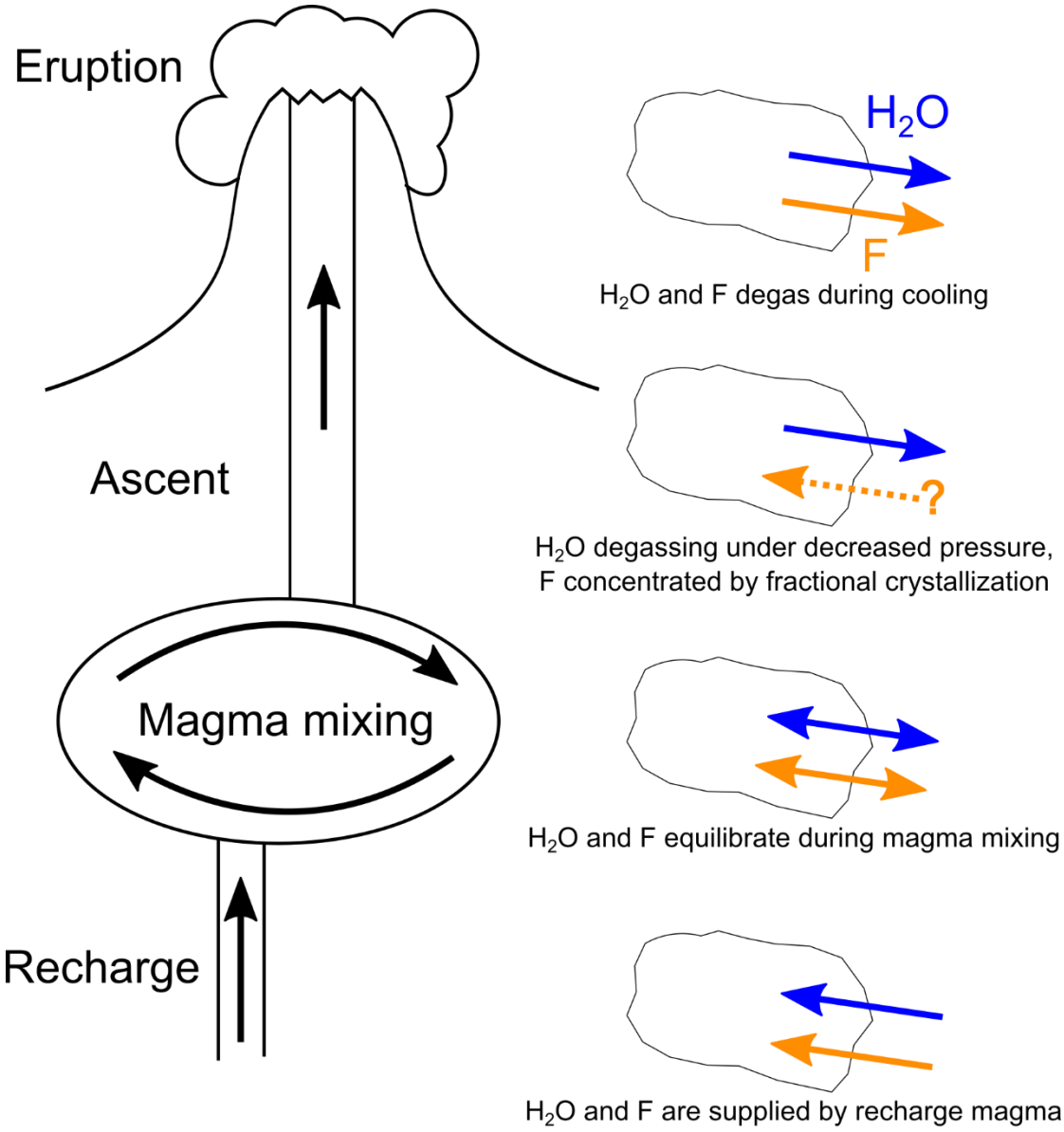

Figure 8. *H_2O and F systematics in Mt. Hood. H_2O and F are supplied by a volatile-rich mafic magma and subsequently equilibrate with the mixed magmas. During ascent and eruption, H_2O in the magma lowers, and plagioclase lose H_2O. F is possibly concentrated by fractional crystallization, leading to F gain. Both H_2O and F may be diffusively lost during prolonged cooling on the surface.*

Bibliography

Aines, R.D., and Rossman, G.R. (1984) Water content of mantle garnets. Geology, 12, 720–723.

Aubaud, C., Withers, A.C., Hirschmann, M.M., Guan, Y., Leshin, L.A., Mackwell, S.J., and Bell, D.R. (2007) Intercalibration of FTIR and SIMS for hydrogen measurements in glasses and nominally anhydrous minerals. American Mineralogist, 92, 811–828.

Balcone-Boissard, H., Villemant, B., and Boudon, G. (2010) Behavior of halogens during the degassing of felsic magmas. Geochemistry, Geophysics, Geosystems, 11.

Bell, D.R., and Rossman, G.R. (1992) Water in Earth's Mantle: The Role of Nominally Anhydrous Minerals. Science, 255, 1391–1397.

Broadley, M.W., Barry, P.H., Ballentine, C.J., Taylor, L.A., and Burgess, R. (2018) End-Permian extinction amplified by plume-induced release of recycled lithospheric volatiles. Nature Geoscience, 11, 682–687.

Caseres, J.R., Mosenfelder, J.L., and Hirschmann, M.M. (2017) Partitioning of hydrogen and fluorine between feldspar and melt under the conditions of lunar crust formation. Lunar and Planetary Sciences Conference, 48, 2303.

Cashman, K. V. (2004) Volatile controls on magma ascent and eruption. In Geophysical Monograph Series Vol. 150, pp. 109–124. International Union of Geodesy and Geophysics;

Cooper, K.M., and Kent, A.J.R. (2014) Rapid remobilization of magmatic crystals kept in cold storage. Nature, 506, 480–3.

Dalou, C., Koga, K.T., Shimizu, N., Boulon, J., and Devidal, J.L. (2012) Experimental determination of F and Cl partitioning between lherzolite and basaltic melt. Contributions to Mineralogy and Petrology, 163, 591–609.

Dasgupta, R., and Dixon, J.E. (2009) Volatiles and volatile-bearing melts in the Earth's interior. Chemical Geology, 262, 1–3.

Demouchy, S., and Mackwell, S. (2006) Mechanisms of hydrogen incorporation and diffusion in iron-bearing olivine. Physics and Chemistry of Minerals, 33, 347–355.

Dingwell, D.B. (1996) Volcanic Dilemma: Flow or Blow? Science, 273, 1054–1055.

Dingwell, D.B., Scarfe, C.M., and Cronin, D.J. (1985) The effect of fluorine on viscosities in the system sodium monoxide-aluminum oxide-silicon dioxide: implications for phonolites, trachytes and rhyolites. American Mineralogist, 70, 80–87.

Dolejš, D., and Zajacz, Z. (2018) Halogens in Silicic Magmas and Their Hydrothermal Systems. In The Role of Halogens in Terrestrial and Extraterrestrial Geochemical

Processes pp. 431–543.

Eppich, G.R., Cooper, K.M., Kent, A.J.R., and Koleszar, A. (2012) Constraints on crystal storage timescales in mixed magmas: Uranium-series disequilibria in plagioclase from Holocene magmas at Mount Hood, Oregon. Earth and Planetary Science Letters, 317–318, 319–330.

Faccenda, M. (2014) Water in the slab: A trilogy. Tectonophysics, 614, 1–30.

Forte, P., and Castro, J.M. (2019) H2O-content and temperature limit the explosive potential of rhyolite magma during Plinian eruptions. Earth and Planetary Science Letters, 506, 157–167.

Gaetani, G.A., and Grove, T.L. (1998) The influence of water on melting of mantle peridotite. Contributions to Mineralogy and Petrology, 131, 323–346.

Grove, T.L., Till, C.B., and Krawczynski, M.J. (2012) The Role of H2O in Subduction Zone Magmatism. Annu. Rev. Earth Planet. Sci, 40, 413–39.

Guggino, S.N., and Hervig, R.L. (2011) Synthesis and Characterization of Five New F-bearing Basalt Reference Materials (Fba Glasses): Quantifying the Fluorine Content of the Basaltic Glass Standards BCR-2G, BHVO-2G. GSA-1G, GSC-1G, GSD-1G, GSE-1G, ML3B-G, KL2-G, and ALV-519-4. AGU Fall Meeting Abstracts, 2535.

Hamada, M., Ushioda, M., Fujii, T., and Takahashi, E. (2013) Hydrogen concentration in plagioclase as a hygrometer of arc basaltic melts: Approaches from melt inclusion analyses and hydrous melting experiments. Earth and Planetary Science Letters, 365, 253–262.

Harris, S.L. (2005) Fire Mountains of the West: The Cascade and Mono Lake Volcanoes, 3rd ed. Mountain Press Publishing Company, Missoula, MT.

Hauri, E.H., Wang, J., Dixon, J.E., King, P.L., Mandeville, C., and Newman, S. (2002) SIMS analysis of volatiles in silicate glasses. Chemical Geology, 183, 99–114.

Hercule, S., and Ingrin, J. (1999) Hydrogen in diopside: Diffusion, kinetics of extraction-incorporation, and solubility. American Mineralogist, 84, 1577–1587.

Hildreth, W. (2007) Quaternary Magmatism in the Cascades - Geologic Perspectives. USGS Professional Paper. U.S. Geological Survey, Reston, VA.

Hirth, G., and Kohlstedt, D.L. (1996) Water in the oceanic upper mantle: implications for rheology, melt extraction and the evolution of the lithosphere. Earth and Planetary Science Letters, 144, 93–108.

Ingrin, J., and Blanchard, M. (2006) Diffusion of Hydrogen in Minerals. Reviews in Mineralogy & Geochemistry, 62, 291–320.

Joachim, B., Pawley, A., Lyon, I.C., Marquardt (neé Hartmann), K., Henkel, T., Clay, P.L., Ruzié, L., Burgess, R., and Ballentine, C.J. (2015) Experimental partitioning of

F and Cl between olivine, orthopyroxene and silicate melt at Earth´s mantle conditions. Chemical Geology.

Johnson, E.A. (2005) Magmatic water contents recorded by hydroxyl concentrations in plagioclase phenocrysts from Mount St. Helens, 1980-1981. Goldschmidt Conference Abstracts 2005, A743, 2005.

Johnson, E.A., and Rossman, G.R. (2003) The concentration and speciation of hydrogen in feldspars using FTIR and H MAS NMR spectroscopy. American Mineralogist, 88, 901–911.

——— (2004) A survey of hydrous species and concentrations in igneous feldspars. American Mineralogist, 89, 586–600.

——— (2012) The diffusion behavior of hydrogen in plagioclase feldspar at 800-1000C: Implications for re-equilibration of hydroxyl in volcanic phenocrysts. American Mineralogist, 98, 1779–1787.

Kent, A.J.R., Darr, C., Koleszar, A.M., Salisbury, M.J., and Cooper, K.M. (2010) Preferential eruption of andesitic magmas through recharge filtering. Nature Geoscience, 3, 631–636.

Kessel, R., Schmidt, M.W., Ulmer, P., and Pettke, T. (2005) Trace element signature of subduction-zone fluids, melts and supercritical liquids at 120-180 km depth. Nature, 437, 724–727.

Koga, K., Hauri, E.H., Hirschmann, M.M., and Bell, D. (2003) Hydrogen concentration analyses using SIMS and FTIR: Comparison and calibration for nominally anhydrous minerals. Geochemistry, Geophysics, Geosystems, 4, 1–20.

Kohlstedt, D.L., and Mackwell, S.J. (1998) Diffusion of Hydrogen and Intrinsic Point Defects in Olivine. Zeitschrift für Physikalische Chemie, 207, 147–162.

Koleszar, A.M., Kent, A.J.R., Wallace, P.J., and Scott, W.E. (2012) Controls on long-term low explosivity at andesitic arc volcanoes: Insights from Mount Hood, Oregon. Journal of Volcanology and Geothermal Research, 219–220, 1–14.

Krawczynski, M.J., Grove, T.L., and Behrens, H. (2012) Amphibole stability in primitive arc magmas: Effects of temperature, H 2O content, and oxygen fugacity. Contributions to Mineralogy and Petrology, 164, 317–339.

Lange, R. a., Frey, H.M., and Hector, J. (2009) A thermodynamic model for the plagioclase-liquid hygrometer/thermometer. American Mineralogist, 94, 494–506.

Lloyd, A.S., Plank, T., Ruprecht, P., Hauri, E.H., and Rose, W. (2013) Volatile loss from melt inclusions in pyroclasts of differing sizes. Contributions to Mineralogy and Petrology, 165, 129–153.

Lloyd, A.S., Ferriss, E., Ruprecht, P., Hauri, E.H., Jicha, B.R., and Plank, T. (2016) An assessment of clinopyroxene as a recorder of magmatic water and magma ascent

rate. Journal of Petrology, 57, 1865–1886.

Marschall, H.R., and Schumacher, J.C. (2012) Arc magmas sourced from mélange diapirs in subduction zones. Nature Geoscience, 5, 862–867.

Mollo, S., Putirka, K.D., Iezzi, G., Del Gaudio, P., and Scarlato, P. (2011) Plagioclase–melt (dis)equilibrium due to cooling dynamics: Implications for thermometry, barometry and hygrometry. Lithos, 125, 221–235.

Mosenfelder, J.L., and Rossman, G.R. (2013) Analysis of hydrogen and fluorine in pyroxenes: I. Orthopyroxene. American Mineralogist, 98, 1042–1054.

Mosenfelder, J.L., Voyer, M. Le, Rossman, G.R., Guan, Y., Bel, D.R., Asimow, P.D., and Eiler, J.M. (2011) Analysis of hydrogen in olivine by SIMS: Evaluation of standards and protocol. American Mineralogist, 96, 1725–1741.

Mosenfelder, J.L., Rossman, G.R., and Johnson, E.A. (2015) Hydrous species in feldspars: A reassessment based on FTIR and SIMS. American Mineralogist, 100, 1209–1221.

O'Leary, J.A., Rossman, G.R., and Eiler, J.M. (2007) Hydrogen analysis in minerals by continuous-flow mass spectrometry. American Mineralogist, 92, 1990–1997.

Plank, T., Kelley, K.A., Zimmer, M.M., Hauri, E.H., and Wallace, P.J. (2013) Why do mafic arc magmas contain ~4wt% water on average? Earth and Planetary Science Letters, 364, 168–179.

Reubi, O., and Blundy, J. (2009) A dearth of intermediate melts at subduction zone volcanoes and the petrogenesis of arc andesites. Nature, 461, 1269–1273.

Roggensack, K., Hervig, R.L., McKnight, S.B., and Williams, S.N. (1997) Explosive Basaltic Volcanism from Cerro Negro Volcano : Influence of Volatiles on Eruptive Style. Science, 277, 1639–1643.

Rosenthal, A., Hauri, E.H., and Hirschmann, M.M. (2015) Experimental determination of C, F, and H partitioning between mantle minerals and carbonated basalt, CO2/Ba and CO2/Nb systematics of partial melting, and the CO2 contents of basaltic source regions. Earth and Planetary Science Letters, 412, 77–87.

Rossman, G.R. (2006) Analytical Methods for Measuring Water in Nominally Anhydrous Minerals. Reviews in Mineralogy and Geochemistry, 62, 1–28.

Ruprecht, P., and Bachmann, O. (2010) Pre-eruptive reheating during magma mixing at Quizapu volcano and the implications for the explosiveness of silicic arc volcanoes. Geology, 38, 919–922.

Rutherford, M.J. (2009) Magma Ascent Rates. Reviews in Mineralogy and Geochemistry, 69, 241–271.

Schmidt, M.W., and Poli, S. (2013) Devolatilization During Subduction, 2nd ed., 669-

701 p. Treatise on Geochemistry: Second Edition Vol. 4. Elsevier Ltd.

Scott, W.E., and Gardner, C.A. (2017) Field-Trip Guide to Mount Hood, Oregon, Highlighting Eruptive History and Hazards. U.S. Geological Survey Scientific Investigations Report 2017 – 5022 – G, 115.

Scott, W.E., Gardner, C.A., Sherrod, D.R., Tilling, R.I., Lanphere, M.A., and Conrey, R.M. (1997a) Geologic History of Mount Hood Volcano, Oregon—A Field-Trip Guidebook. US Geological Survey Open-File Report, 97, 38p.

Scott, W.E., Pierson, T.C., Schilling, S.P., Costa, J.E., Gardner, C.A., Vallance, J.W., and Major, J.J. (1997b) Volcano Hazards in the Mount Hood Region, Oregon. US Geological Survey Open-File Report, 1–14.

Seaman, S.J., Dyar, M.D., Marinkovic, N., and Dunbar, N.W. (2006) An FTIR study of hydrogen in anorthoclase and associated melt inclusions. American Mineralogist, 91, 12–20.

Singer, B.S., Myers, J.D., and Frost, C.D. (1992) Mid-Pleistocene lavas from the Seguam volcanic center, central Aleutian arc: closed-system fractional crystallization of a basalt to rhyodacite eruptive suite. Contributions to Mineralogy and Petrology, 110, 87–112.

Straub, S.M., and Layne, G.D. (2003) The systematics of chlorine, fluorine, and water in Izu arc front volcanic rocks: Geochimica et Cosmochimica Acta, 67, 4179–4203.

Sweeney, R.J., Prozesky, V.M., and Springhorn, K.A. (1997) Use of the elastic recoil detection analysis (ERDA) microbeam technique for the quantitative determination of hydrogen in materials and hydrogen partitioning between olivine and melt at high pressures. Geochimica et Cosmochimica Acta, 61, 101–113.

Tenner, T.J., Hirschmann, M.M., Withers, A.C., and Hervig, R.L. (2009) Hydrogen partitioning between nominally anhydrous upper mantle minerals and melt between 3 and 5 GPa and applications to hydrous peridotite partial melting. Chemical Geology, 262, 42–56.

Van Keken, P.E., Hacker, B.R., Syracuse, E.M., and Abers, G.A. (2011) Subduction factory: 4. Depth-dependent flux of H2O from subducting slabs worldwide. Journal of Geophysical Research: Solid Earth, 116.

Vermeesch, P. (2018) IsoplotR: A free and open toolbox for geochronology. Geoscience Frontiers.

Wade, J.A., Plank, T., Hauri, E.H., Kelley, K.A., Roggensack, K., and Zimmer, M. (2008) Prediction of magmatic water contents via measurement of H2O in clinopyroxene phenocrysts. Geology, 36, 799–802.

Wallace, P.J. (2005) Volatiles in subduction zone magmas: Concentrations and fluxes based on melt inclusion and volcanic gas data. Journal of Volcanology and Geothermal Research, 140, 217–240.

Wallace, P.J., and Anderson, A.T. (2000) Volatiles in magmas. In Encylopedia of Volcanoes pp. 149–170.

Waters, L.E., and Lange, R.A. (2015) An updated calibration of the plagioclase-liquid hygrometer-thermometer applicable to basalts through rhyolites. American Mineralogist, 100, 2172–2184.

Webster, J.D., Baker, D.R., and Aiuppa, A. (2018) Halogens in Mafic and Intermediate-Silica Content Magmas. In The Role of Halogens in Terrestrial and Extraterrestrial Geochemical Processes pp. 307–430.

Woods, S.C., Mackwell, S., and Dyar, D. (2000) Hydrogen in diopside: Diffusion profiles. American Mineralogist, 85, 480–487.

Wright, H.M., Bacon, C.R., Vazquez, J.A., and Sisson, T.W. (2012) Sixty thousand years of magmatic volatile history before the caldera-forming eruption of Mount Mazama, Crater Lake, Oregon. Contributions to Mineralogy and Petrology, 164, 1027–1052.

Wyllie, P.J. (1979) Magmas and volatile components. American Mineralogist, 64, 469–500.

Yang, X. (2012) An experimental study of H solubility in feldspars: Effect of composition, oxygen fugacity, temperature and pressure and implications for crustal processes. Geochimica et Cosmochimica Acta, 97, 46–57.

Yang, X., Keppler, H., and Li, Y. (2016) Molecular hydrogen in mantle minerals. Geochemical Perspectives Letters, 160–168.

York, D. (1966) Least-squares fitting of a straight line. Canadian Journal of Physics, 44, 1079–1086.

Appendix A: BSE images and SIMS maps of all phenocrysts in this study

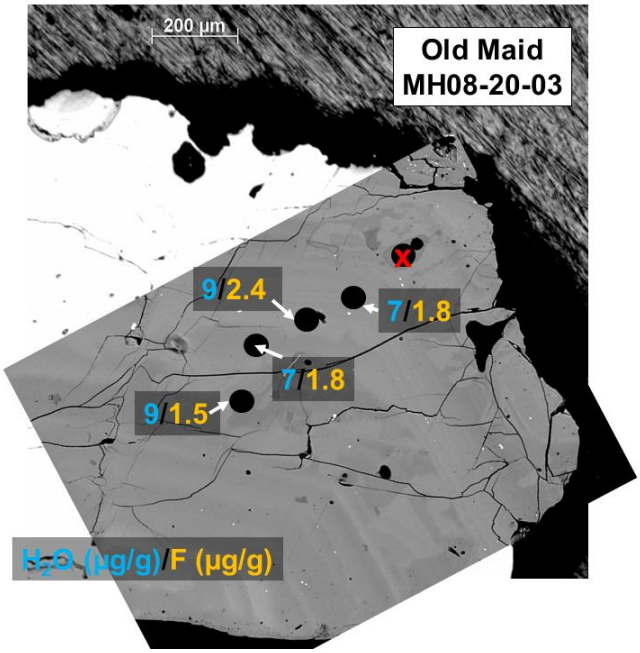

Coordinate data lost for MH08-20-04, data recorded in Appendix B.

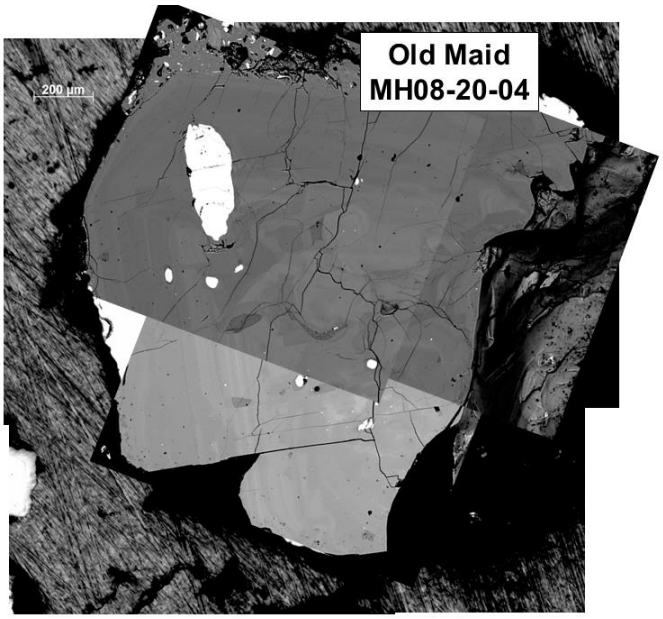

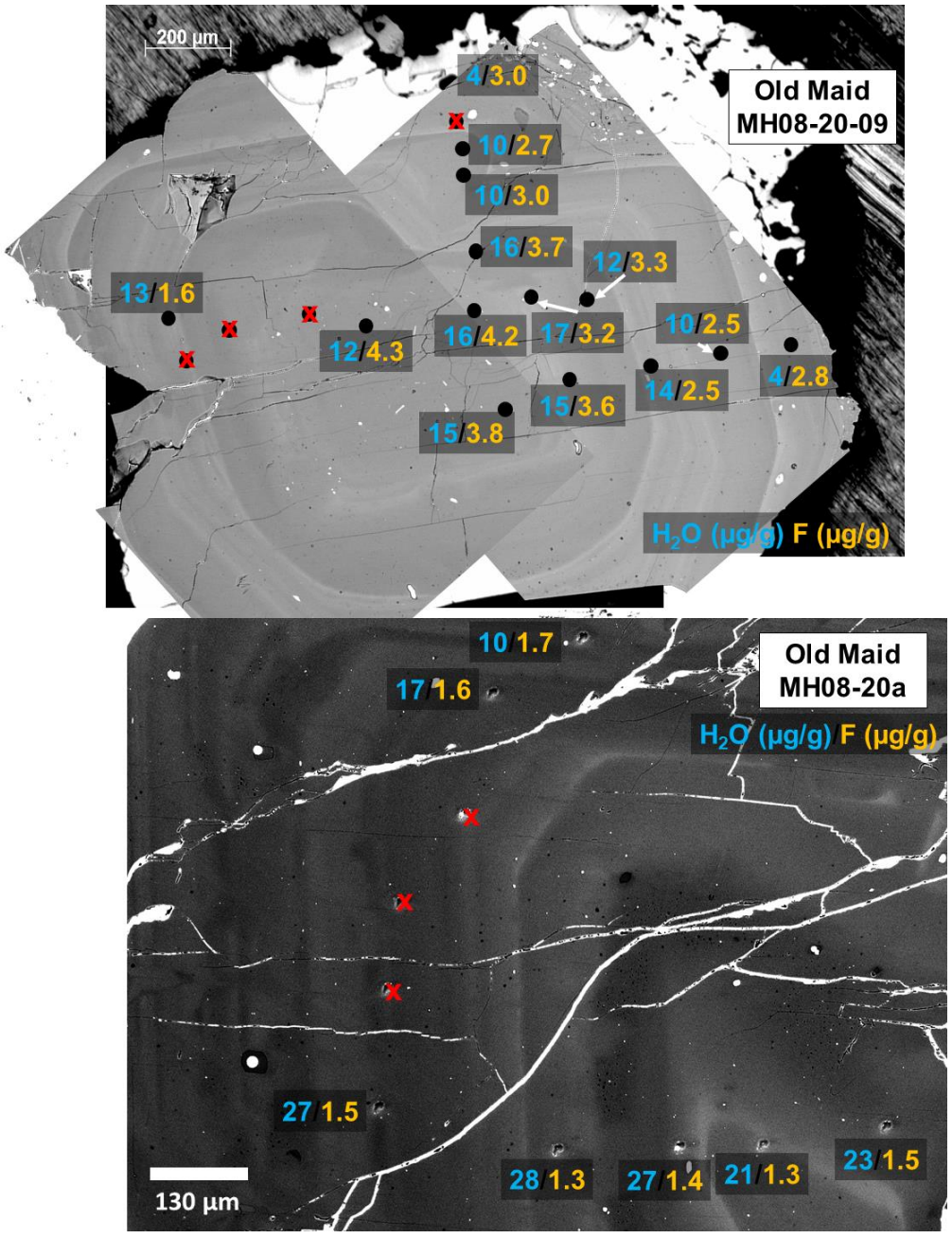
200 µm
4/3.0
Old Maid
MH08-20-09
10/2.7
10/3.0
16/3.7
12/3.3
13/1.6
16/4.2
17/3.2
10/2.5
12/4.3
4/2.8
14/2.5
15/3.6
15/3.8
H2O (µg/g) F (µg/g)
10/1.7
Old Maid
MH08-20a
17/1.6
H2O (µg/g) F (µg/g)
27/1.5
130 µm
28/1.3
27/1.4
21/1.3
23/1.5

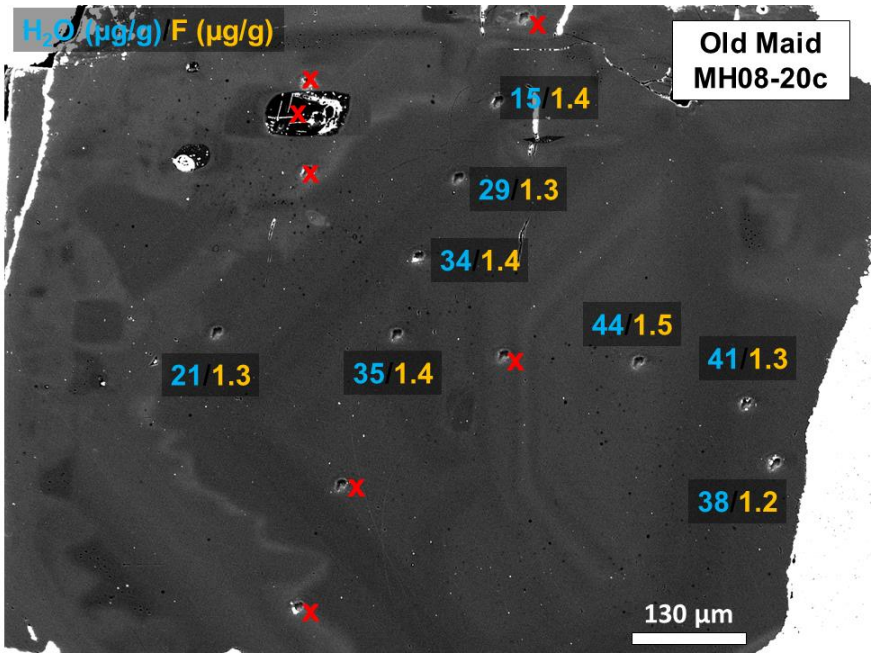
H2O (µg/g) F (µg/g)
Old Maid
MH08-20c
15/1.4
29/1.3
34/1.4
44/1.5
41/1.3
21/1.3
35/1.4
38/1.2
130 µm

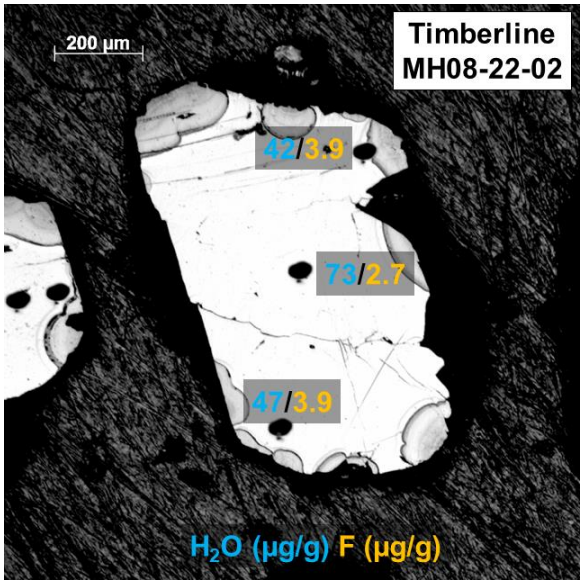
200 µm
Timberline
MH08-22-02
42/3.9
73/2.7
47/3.9
H2O (µg/g) F (µg/g)

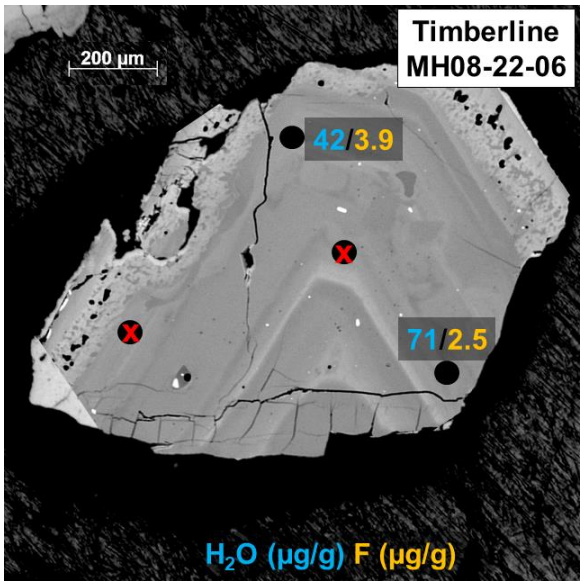
200 µm
Timberline
MH08-22-06
42/3.9
71/2.5
H2O (µg/g) F (µg/g)

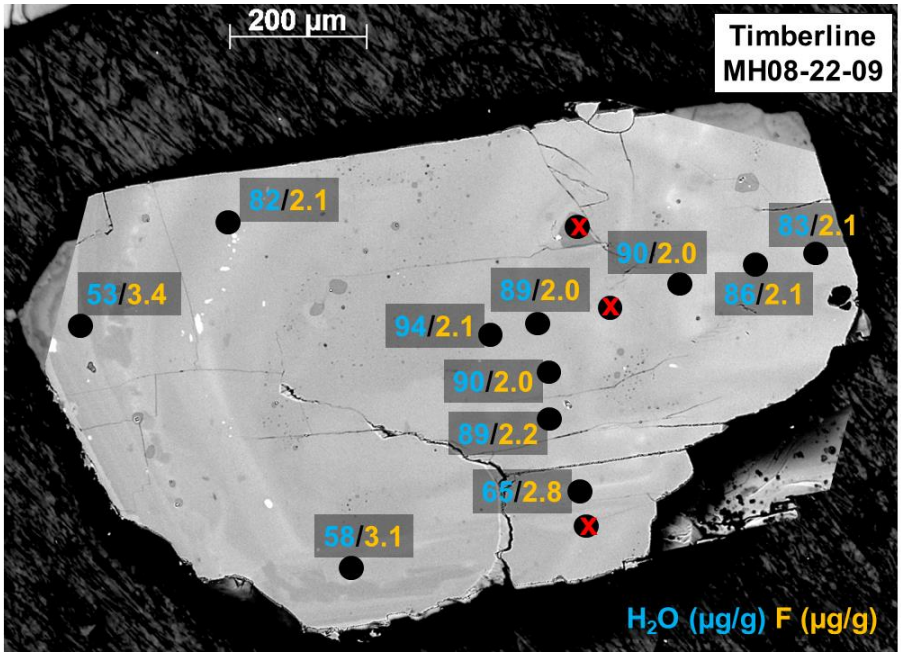
200 µm
Timberline
MH08-22-09
82/2.1
83/2.1
90/2.0
53/3.4
89/2.0
86/2.1
94/2.1
90/2.0
89/2.2
66/2.8
58/3.1
H2O (µg/g) F (µg/g)

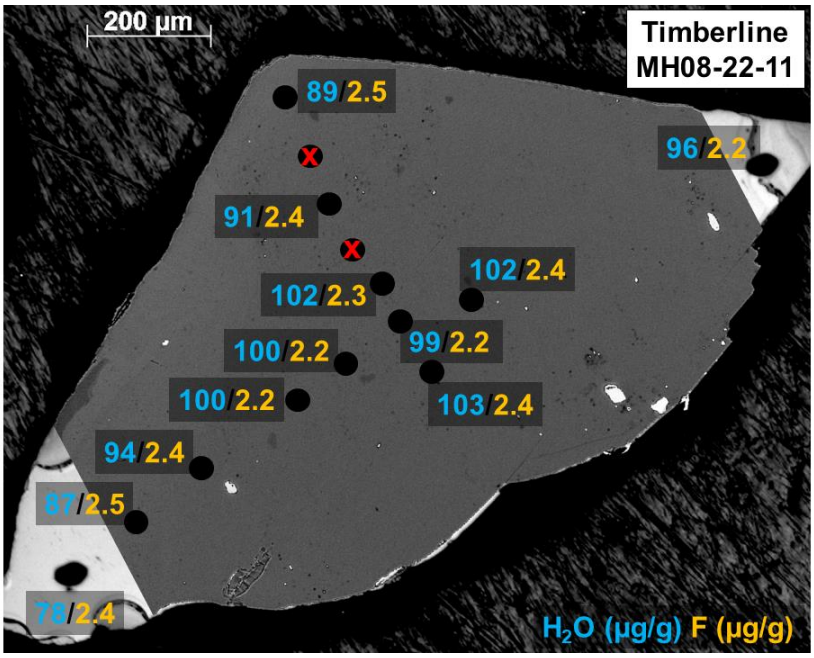
200 µm
Timberline
MH08-22-11
89/2.5
96/2.2
91/2.4
102/2.4
102/2.3
99/2.2
100/2.2
100/2.2
103/2.4
94/2.4
87/2.5
78/2.4
H2O (µg/g) F (µg/g)

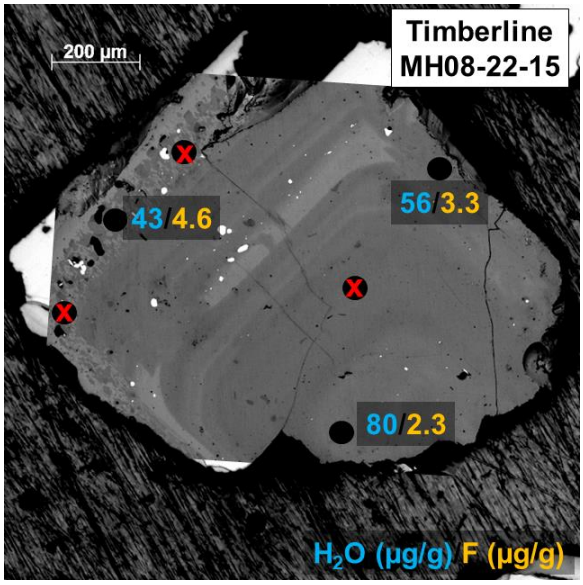
200 µm
Timberline
MH08-22-15
56/3.3
43/4.6
80/2.3
H2O (µg/g) F (µg/g)

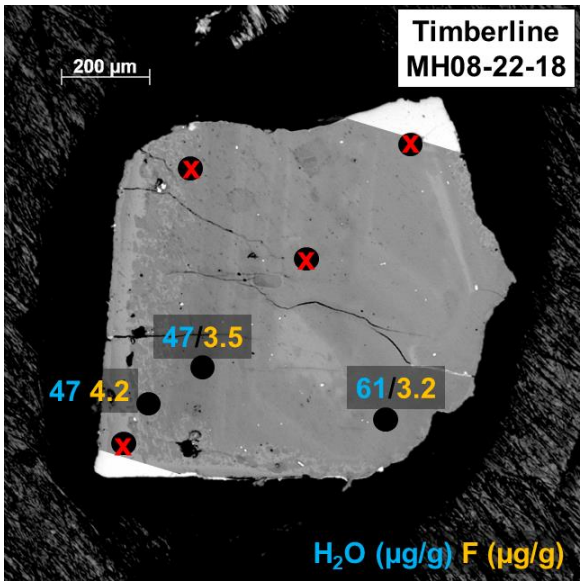
Timberline
MH08-22-18
200 µm
47 3.5
47 4.2
61 3.2
H2O (µg/g) F (µg/g)

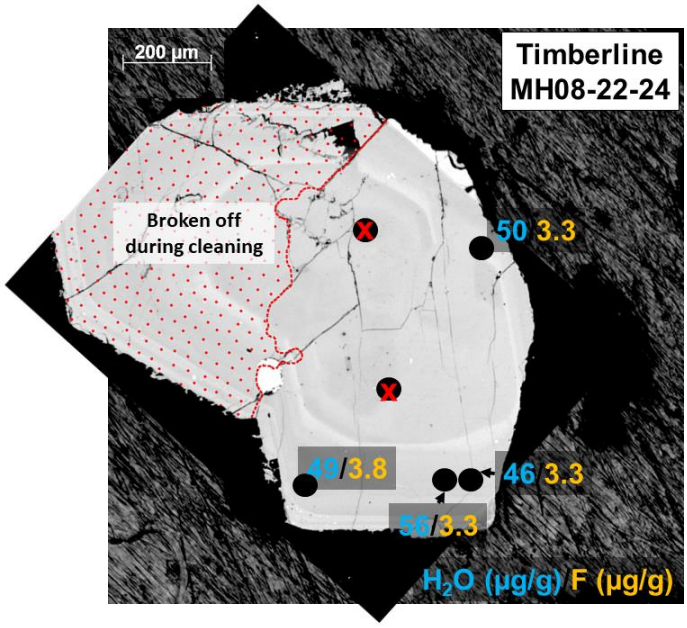
Timberline
MH08-22-24
200 µm
Broken off
during cleaning
50 3.3
49 3.8
46 3.3
56 3.3
H2O (µg/g) F (µg/g)

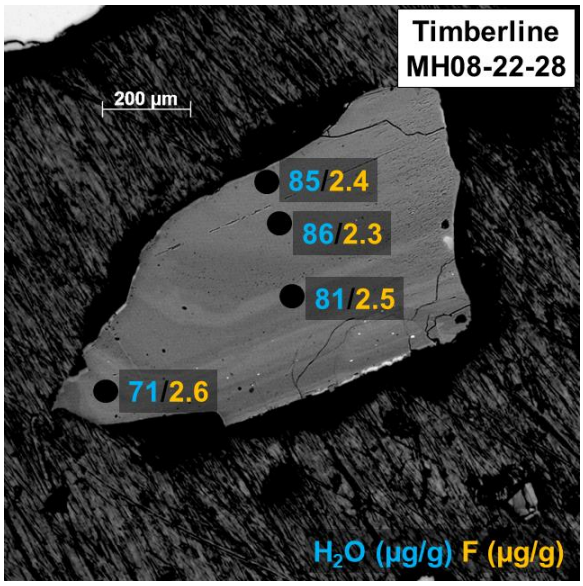
Timberline
MH08-22-28
200 µm
85/2.4
86/2.3
81/2.5
71/2.6
H2O (µg/g) F (µg/g)

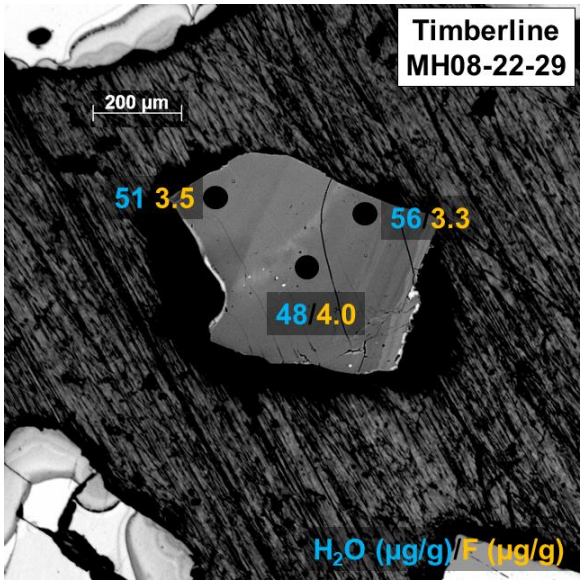
Timberline
MH08-22-29
200 µm
51 3.5
56 3.3
48/4.0
H2O (µg/g) F (µg/g)

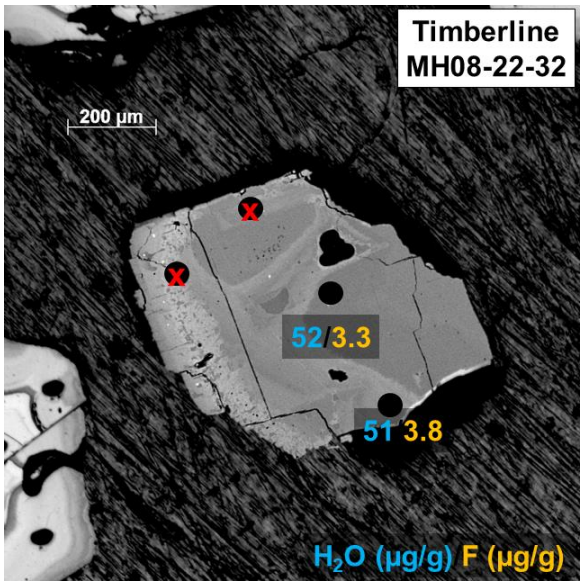
Timberline
MH08-22-32
200 µm
52/3.3
51/3.8
H2O (µg/g) F (µg/g)

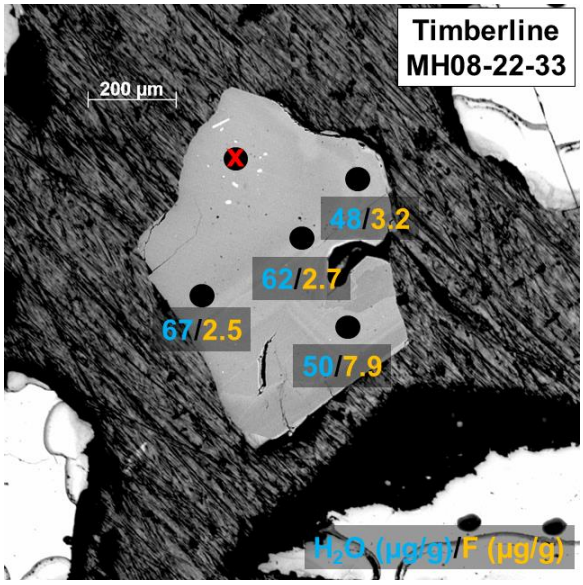
Timberline
MH08-22-33
200 µm
48/3.2
62/2.7
67/2.5
50/7.9
H2O (µg/g) F (µg/g)

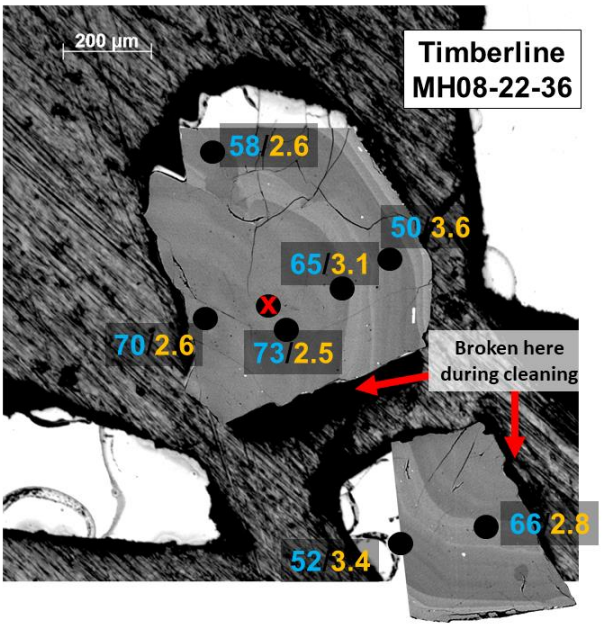
200 µm
Timberline
MH08-22-36
58 2.6
50 3.6
65 3.1
70 2.6
73 2.5
Broken here
during cleaning
66 2.8
52 3.4

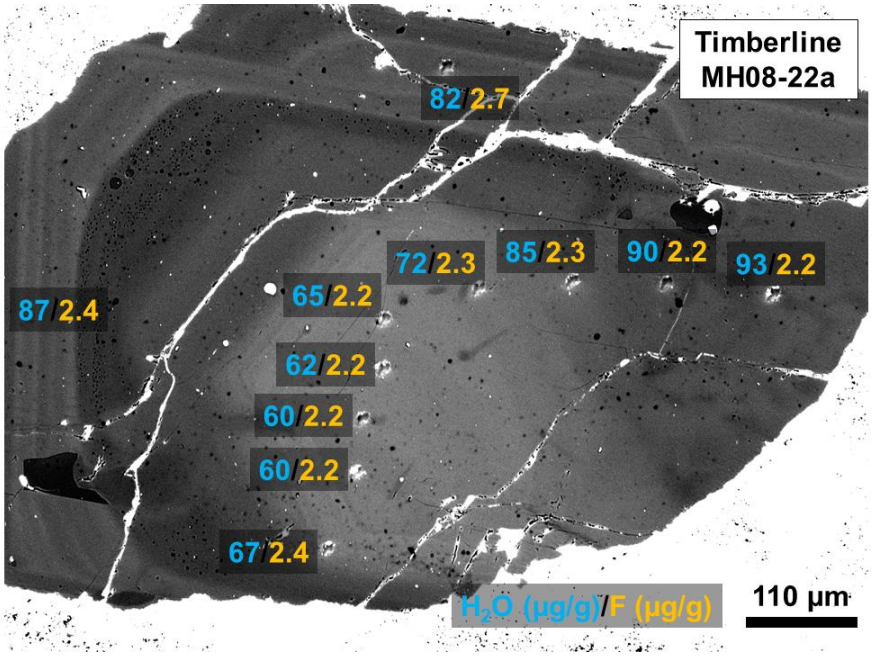
Timberline
MH08-22a
82 2.7
72 2.3
85 2.3
90 2.2
93 2.2
87 2.4
65 2.2
62 2.2
60 2.2
60 2.2
67 2.4
H2O (µg/g)/F (µg/g)
110 µm

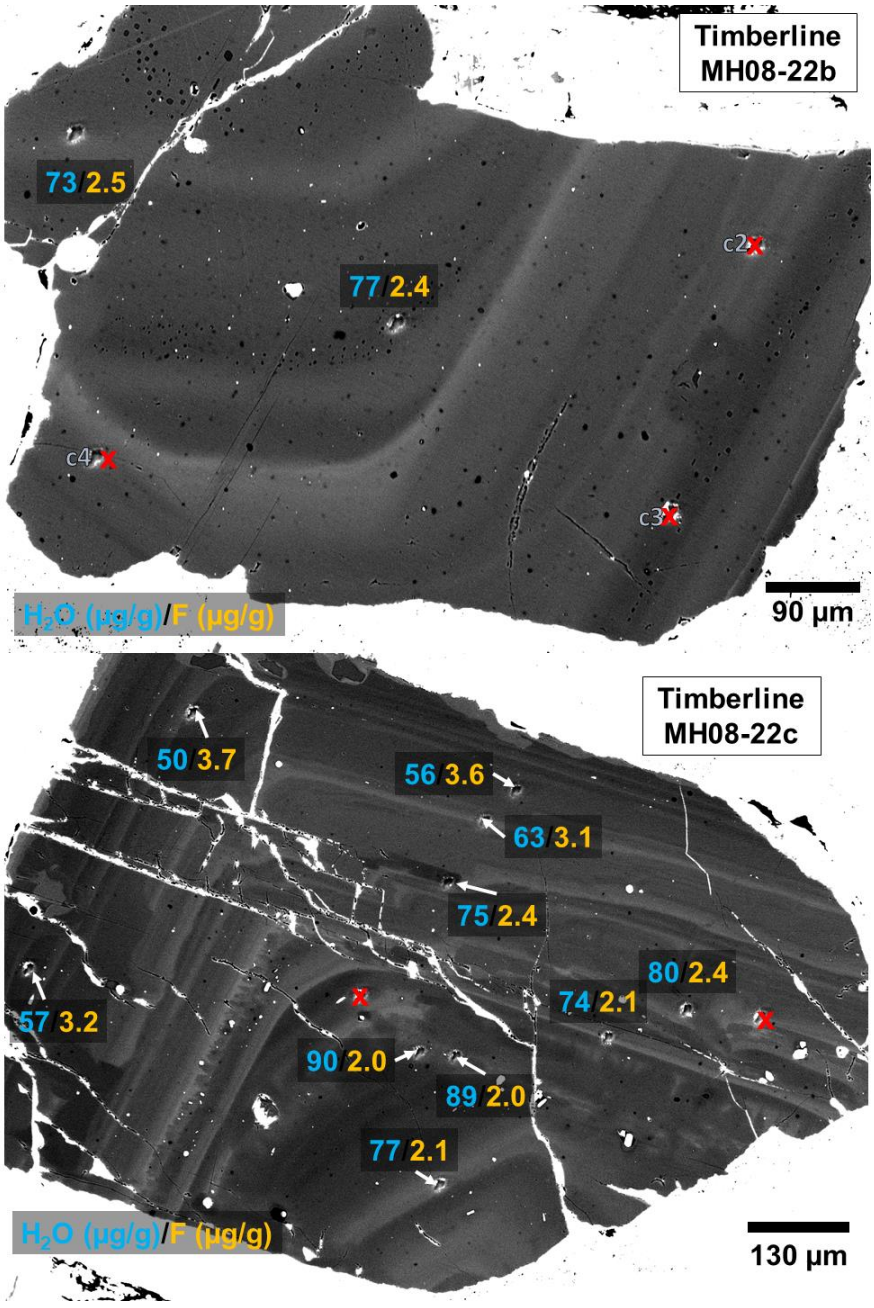
Timberline
MH08-22b
73 2.5
77 2.4
c2
c4
c3
H2O (µg/g)/F (µg/g)
90 µm
Timberline
MH08-22c
50 3.7
56 3.6
63 3.1
75 2.4
80 2.4
74 2.1
57 3.2
90 2.0
89 2.0
77 2.1
H2O (µg/g)/F (µg/g)
130 µm


Timberline
MH08-22d
89 2.3
101 1.9
86 2.4
91 1.9
H2O (µg/g)/F (µg/g)
130 µm

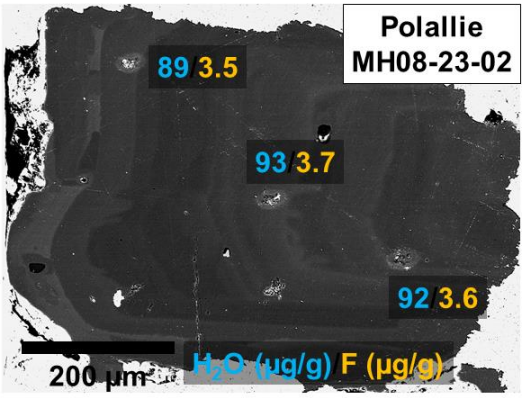
Polallie
MH08-23-02
89 3.5
93 3.7
92 3.6
200 µm
H2O (µg/g) F (µg/g)

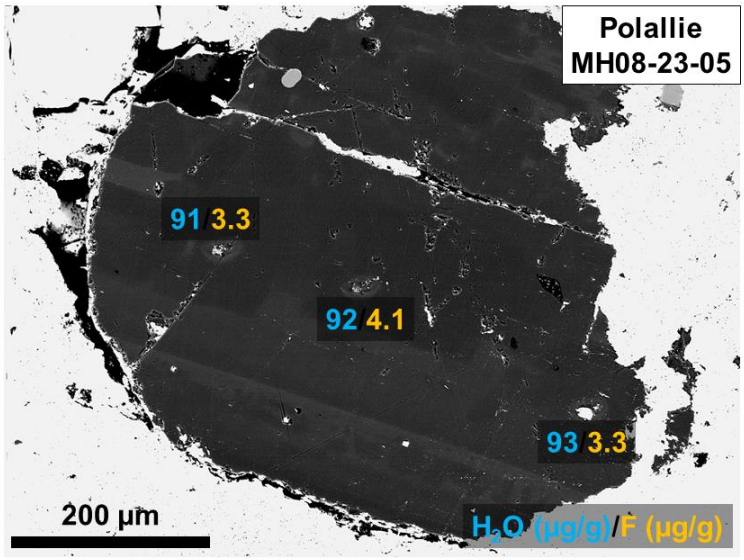
Polallie
MH08-23-05
91 3.3
92 4.1
93 3.3
200 µm
H2O (µg/g)/F (µg/g)

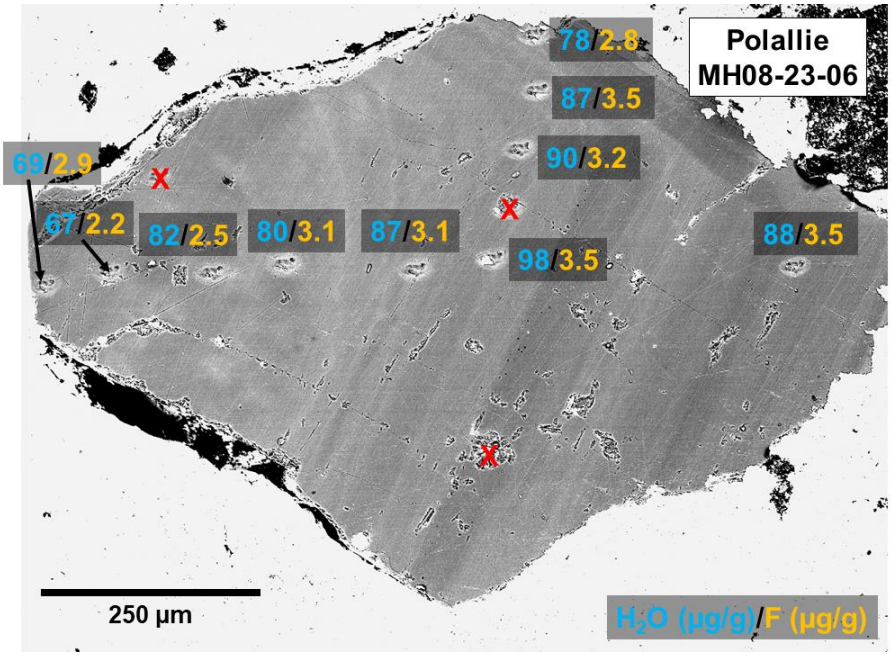
Polallie
MH08-23-06
78/2.8
87/3.5
90/3.2
69/2.9
67/2.2
82/2.5
80/3.1
87/3.1
98/3.5
88/3.5
250 µm
H2O (µg/g)/F (µg/g)

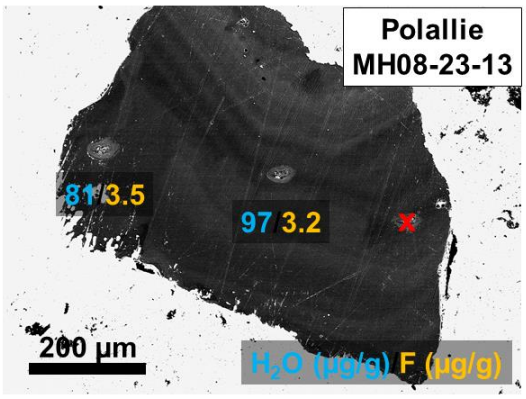
Polallie
MH08-23-13
81/3.5
97/3.2
200 µm
H2O (µg/g) F (µg/g)

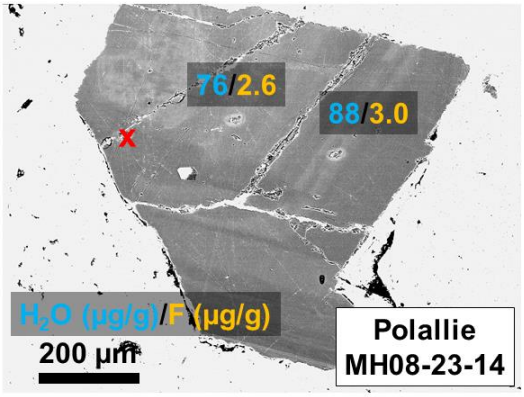
76/2.6
88/3.0
H2O (µg/g)/F (µg/g)
200 µm
Polallie
MH08-23-14

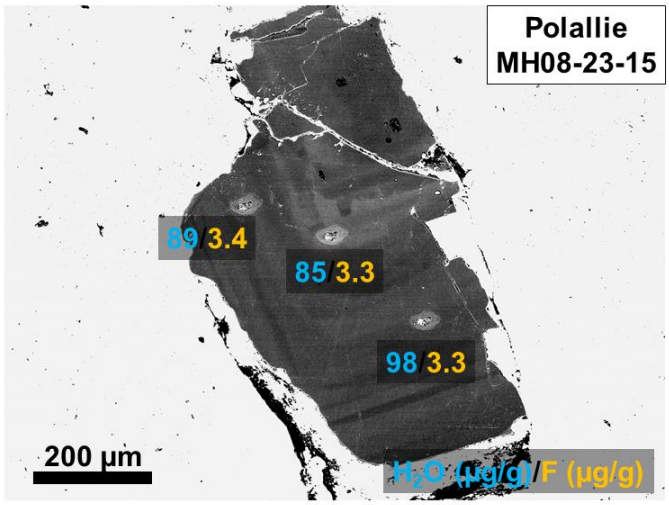
Polallie
MH08-23-15
89/3.4
85/3.3
98 3.3
200 µm
H2O (µg/g)/F (µg/g)

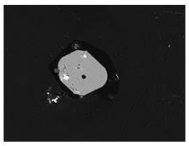

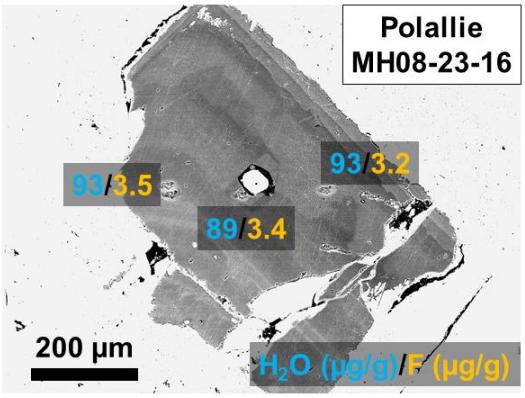
Polallie
MH08-23-16
93/3.2
93/3.5
89/3.4
200 µm
H2O (µg/g)/F (µg/g)

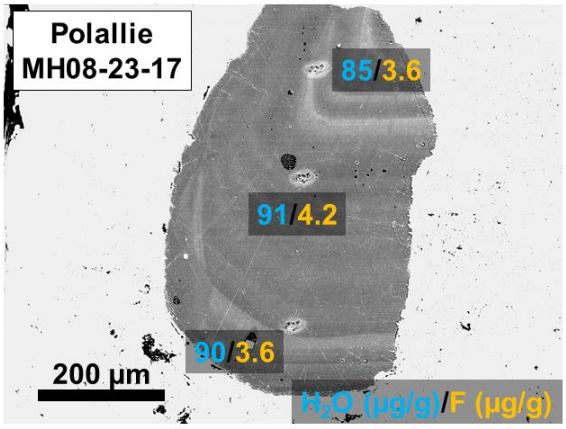
Polallie
MH08-23-17
85/3.6
91/4.2
90/3.6
200 µm
H2O (µg/g)/F (µg/g)

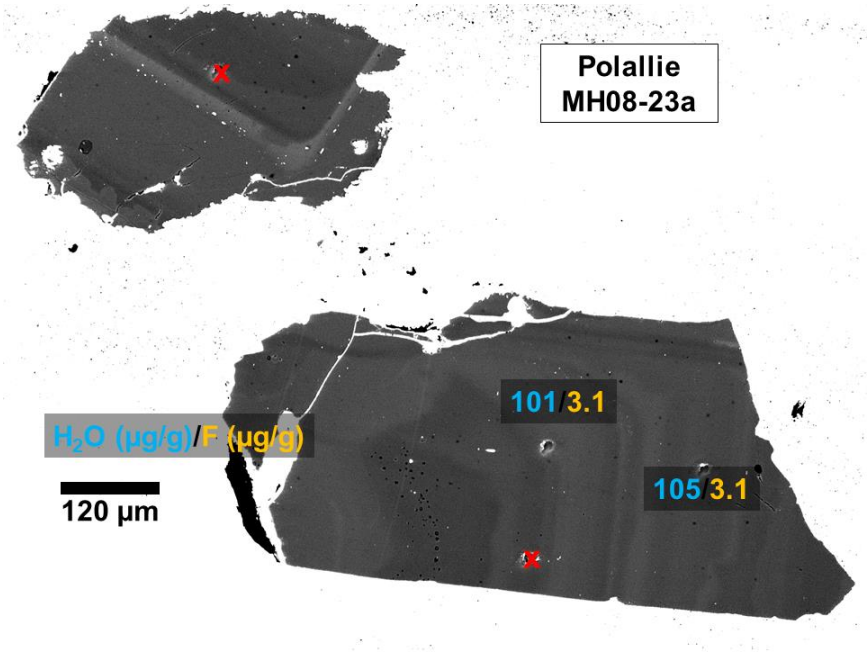
Polallie
MH08-23a
101/3.1
105/3.1
H2O (µg/g)/F (µg/g)
120 µm

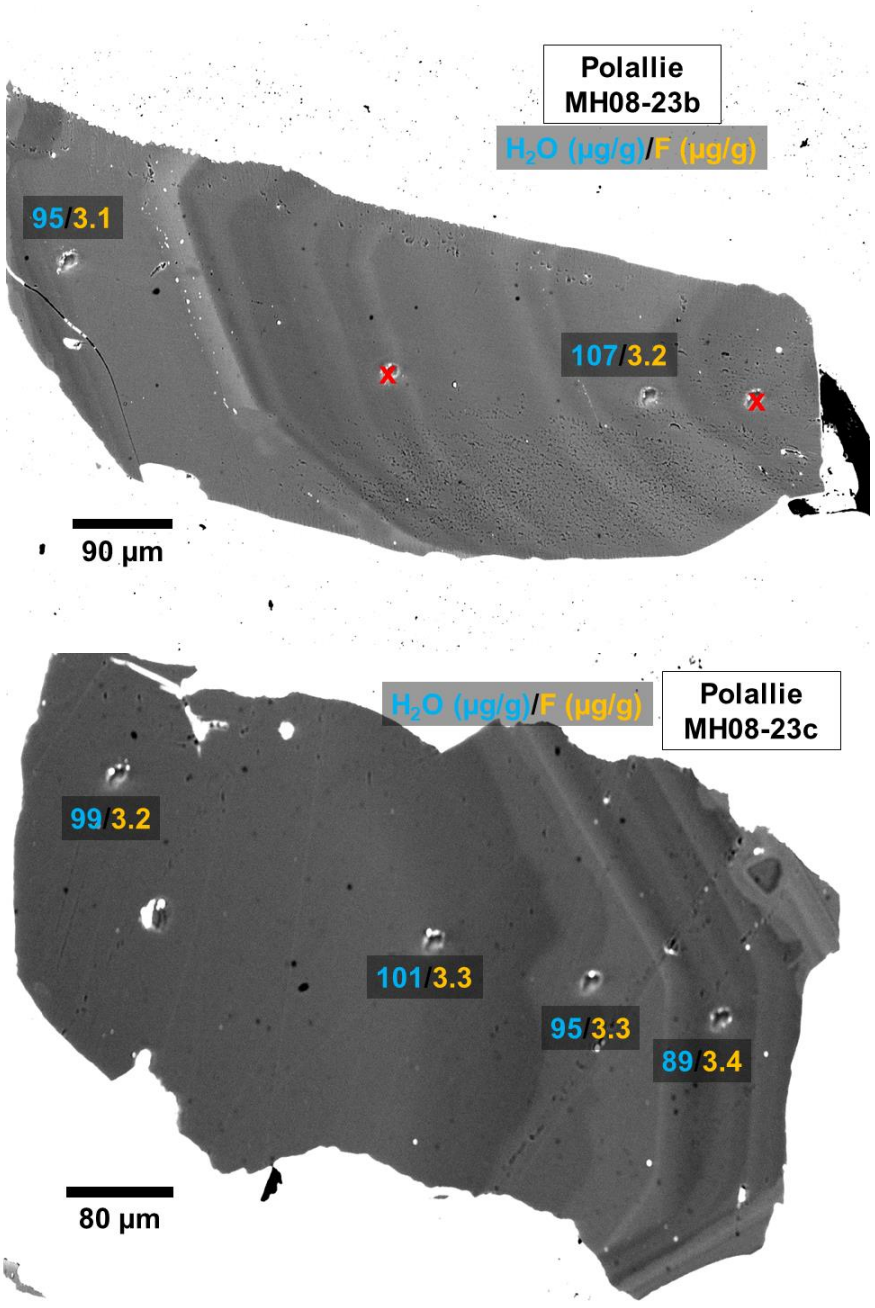
Polallie
MH08-23b
H2O (µg/g)/F (µg/g)
95/3.1
107/3.2
90 µm
H2O (µg/g)/F (µg/g)
Polallie
MH08-23c
99/3.2
101/3.3
95/3.3
89/3.4
80 µm

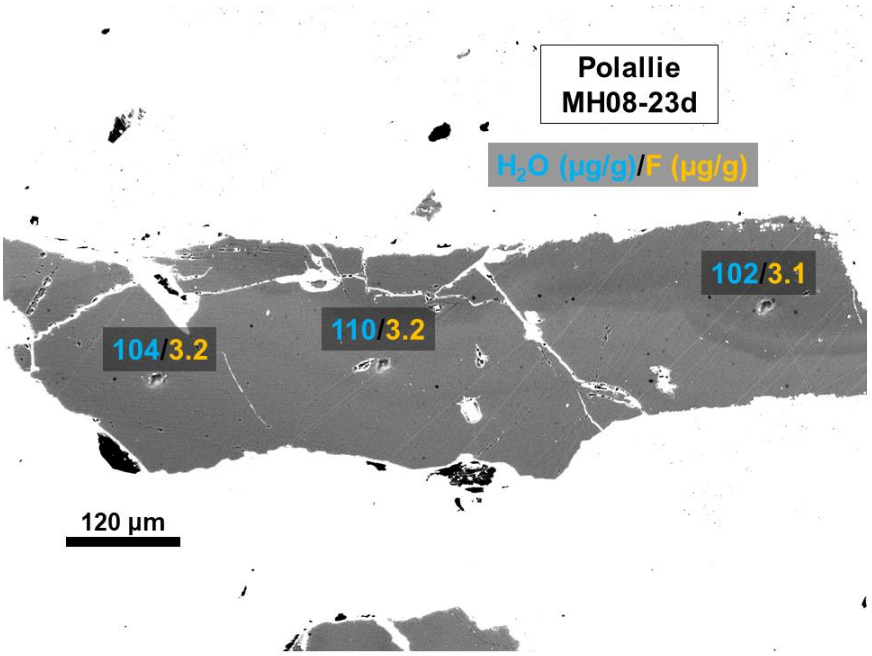
Polallie
MH08-23d
H2O (µg/g)/F (µg/g)
102/3.1
110/3.2
104/3.2
120 µm

Appendix B: Summaries of SIMS analyses

Each analysis (filename) with calculated H2O and F from blank corrected 16O1H/18O and 19F/18O. Poisson ratio is $\sigma_{mean}/\sigma_{Poisson}$.

Filename	Sample No.	Eruptive unit	H_2O µg/g	± 2s	F µg/g	± 2s	^{12}C, cps	± $2s_{mean}$	$^{16}O^{1}H/^{18}O$, blank corrected	$s_{mean}/s_{Poisson}$ [$^{16}O^{1}H/^{18}O$]	$^{19}F/^{18}O$, blank corrected	$s_{mean}/s_{Poisson}$ [$^{19}F/^{18}O$]
MH0822chain1@0.asc	MH08-22d	Timberline	91	6	1.9	0.2	5.1	0.4	0.0147	1.15	0.0045	0.83
MH0822chain1@1.asc	MH08-22b	Timberline	77	6	2.4	0.4	7.6	1.1	0.0125	1.26	0.0057	1.25
MH0822chain1@5.asc	MH08-22b	Timberline	73	4	2.5	0.4	8.4	0.9	0.0118	0.97	0.0062	1.09
MH0822chain1@8.asc	MH08-22c	Timberline	77	4	2.1	0.3	7.3	0.6	0.0124	0.98	0.0051	0.97
MH0822chain1@9.asc	MH08-22c	Timberline	50	3	3.7	0.3	6.1	0.6	0.0080	0.98	0.0089	0.82
MH0822chain1@10.asc	MH08-22c	Timberline	57	3	3.2	0.3	6.1	0.6	0.0091	0.69	0.0078	0.87
mh08weds@1.asc	MH08-22c	Timberline	56	5	3.6	0.5	8.3	3.0	0.0089	1.22	0.0086	1.25
mh08weds@2.asc	MH08-22c	Timberline	75	6	2.4	0.4	4.5	0.8	0.0121	1.22	0.0059	1.06
mh08weds@3.asc	MH08-22c	Timberline	63	5	3.1	0.4	3.6	0.6	0.0101	1.20	0.0075	1.00
mh08weds@4.asc	MH08-20d	Old Maid	11	2	1.3	0.2	4.8	0.6	0.0016	1.00	0.0031	0.90
mh08weds@11.asc	MH08-20d	Old Maid	16	3	1.8	0.2	4.8	0.7	0.0024	1.45	0.0042	0.78
mh08weds@12.asc	MH08-20d	Old Maid	6	2	2.7	0.3	7.4	0.8	0.0008	1.20	0.0065	0.81
mh08weds@14.asc	MH08-20a	Old Maid	13	2	1.7	0.2	7.5	1.5	0.0020	1.17	0.0042	0.89
mh08weds@15.asc	MH08-20a	Old Maid	23	2	1.5	0.3	6.5	0.8	0.0035	0.92	0.0037	1.24
mh08weds@19.asc	MH08-22a	Timberline	65	4	2.2	0.3	5.3	0.7	0.0105	0.94	0.0053	1.07
mh08weds@20.asc	MH08-22a	Timberline	87	5	2.4	0.4	6.8	0.9	0.0141	1.12	0.0058	1.11
mh08weds_chain1.asc	MH08-22c	Timberline	80	5	2.4	0.3	5.5	0.8	0.0129	1.05	0.0059	0.99
mh08weds_chain1@0.asc	MH08-22c	Timberline	74	4	2.1	0.3	5.4	0.5	0.0120	1.01	0.0052	1.08

Filename	Sample No.	Eruptive unit	H_2O µg/g	± 2s	F µg/g	± 2s	^{12}C, cps	± $2s_{mean}$	$^{16}O^{1}H/^{18}O$, blank corrected	$s_{mean}/s_{Poisson}$ [$^{16}O^{1}H/^{18}O$]	$^{19}F/^{18}O$, blank corrected	$s_{mean}/s_{Poisson}$ [$^{19}F/^{18}O$]
MH0822chain1@0.asc	MH08-22d	Timberline	91	6	1.9	0.2	5.1	0.4	0.0147	1.15	0.0045	0.83
mh08weds_chain1@1.asc	MH08-22c	Timberline	89	4	2.0	0.4	4.1	0.7	0.0143	0.83	0.0049	1.20
mh08weds_chain1@2.asc	MH08-22c	Timberline	90	4	2.0	0.2	3.8	0.7	0.0146	0.76	0.0049	0.80
mh08weds_chain1@3.asc	MH08-22a	Timberline	93	5	2.2	0.3	4.5	0.8	0.0150	1.03	0.0054	0.95
mh0823.asc	MH08-23a	Polallie	101	5	3.1	0.3	5.9	0.9	0.0163	0.95	0.0075	0.89
mh0823@1.asc	MH08-23a	Polallie	105	6	3.1	0.4	5.3	0.7	0.0169	1.08	0.0074	1.04
mh0823@5.asc	MH08-23b	Polallie	95	4	3.1	0.3	8.5	0.8	0.0154	0.77	0.0075	1.03
mh0823@7.asc	MH08-23b	Polallie	107	7	3.2	0.4	7.5	0.8	0.0174	1.20	0.0077	1.16
mh0823@8.asc	MH08-23c	Polallie	101	7	3.3	0.4	5.7	0.8	0.0163	1.26	0.0079	1.17
mh0823@9.asc	MH08-23c	Polallie	99	7	3.2	0.4	7.1	0.9	0.0160	1.26	0.0077	1.14
mh0823@10.asc	MH08-23c	Polallie	89	6	3.4	0.4	3.9	0.5	0.0144	1.14	0.0083	0.96
mh0823@11.asc	MH08-23c	Polallie	95	5	3.3	0.4	3.5	0.8	0.0154	0.88	0.0081	0.95
mh0823@12.asc	MH08-23d	Polallie	110	9	3.2	0.5	7.2	0.6	0.0178	1.69	0.0077	1.22
mh0823@13.asc	MH08-23d	Polallie	104	6	3.2	0.3	7.6	1.0	0.0169	1.15	0.0077	0.84
mh0823@14.asc	MH08-23d	Polallie	102	6	3.1	0.3	5.7	0.7	0.0166	1.06	0.0074	0.84
mh0823@16.asc	MH08-22a	Timberline	82	6	2.7	0.3	3.6	0.6	0.0133	1.22	0.0064	0.93
mh0823@17.asc	MH08-22a	Timberline	62	4	2.2	0.2	4.7	0.7	0.0100	1.01	0.0052	0.65
mh0822a_thurs.asc	MH08-22a	Timberline	90	5	2.2	0.3	4.6	0.7	0.0146	1.09	0.0053	1.10
mh0822a_thurs@0.asc	MH08-22a	Timberline	85	5	2.3	0.3	5.1	0.9	0.0137	0.96	0.0056	0.87
mh0822a_thurs@1.asc	MH08-22a	Timberline	72	6	2.3	0.3	5.3	0.7	0.0115	1.27	0.0055	1.00
mh0822a_thurs@2.asc	MH08-22a	Timberline	60	4	2.2	0.4	7.4	1.9	0.0097	0.99	0.0054	1.34

Filename	Sample No.	Eruptive unit	H_2O µg/g	± 2s	F µg/g	± 2s	^{12}C, cps	± $2s_{mean}$	$^{16}O^1H/^{18}O$, blank corrected	$s_{mean}/s_{Poisson}$ [$^{16}O^1H/^{18}O$]	$^{19}F/^{18}O$, blank corrected	$s_{mean}/s_{Poisson}$ [$^{19}F/^{18}O$]
MH0822chain1@0.asc	MH08-22d	Timberline	91	6	1.9	0.2	5.1	0.4	0.0147	1.15	0.0045	0.83
mh0822a_thurs@3.asc	MH08-22a	Timberline	60	7	2.2	0.4	5.1	1.1	0.0097	1.78	0.0053	1.16
mh0822a_thurs@4.asc	MH08-22a	Timberline	67	4	2.4	0.3	6.0	1.7	0.0108	0.95	0.0057	1.07
mh08_thurs@2.asc	MH08-20c	Old Maid	35	3	1.4	0.3	4.0	0.6	0.0056	1.02	0.0033	1.11
mh08_thurs@3.asc	MH08-20c	Old Maid	41	3	1.3	0.2	4.4	0.5	0.0065	0.94	0.0032	0.95
mh08_thurs@5.asc	MH08-20c	Old Maid	38	3	1.2	0.2	5.1	0.8	0.0061	0.94	0.0029	0.96
mh0820c_thurs.asc	MH08-20c	Old Maid	21	2	1.3	0.2	9.0	0.9	0.0033	0.94	0.0031	0.90
mh0820c_thurs@1.asc	MH08-20c	Old Maid	44	3	1.5	0.3	3.8	0.5	0.0070	0.79	0.0036	1.15
mh0820c_thurs@2.asc	MH08-20c	Old Maid	15	1	1.4	0.2	8.1	1.1	0.0023	0.72	0.0034	0.71
mh0820c_thurs@3.asc	MH08-20c	Old Maid	29	2	1.3	0.3	2.8	0.5	0.0045	0.82	0.0032	1.07
mh0820c_thurs@4.asc	MH08-20c	Old Maid	34	3	1.4	0.3	7.8	1.1	0.0053	1.01	0.0033	1.23
mh0820a_thurs.asc	MH08-20a	Old Maid	21	2	1.3	0.2	4.0	0.5	0.0033	0.98	0.0032	0.97
mh0820a_thurs@0.asc	MH08-20a	Old Maid	27	3	1.4	0.2	3.5	0.7	0.0043	0.96	0.0033	0.93
mh0820a_thurs@1.asc	MH08-20a	Old Maid	28	3	1.3	0.2	3.8	0.7	0.0045	1.07	0.0031	0.85
mh0820a_thurs@2.asc	MH08-20a	Old Maid	27	3	1.5	0.2	6.2	0.8	0.0042	1.01	0.0037	0.72
mh0820a_thurs@5.asc	MH08-20a	Old Maid	17	2	1.6	0.3	3.2	0.6	0.0026	1.03	0.0039	1.12
MH0822@1.asc	MH08-22d	Timberline	3	1	6.8	0.6	8.1	1.3	0.0176	0.00	0.0003	1.06
MH0822@3.asc	MH08-22d	Timberline	3	1	6.7	0.6	8.8	1.1	0.0174	0.00	0.0003	1.22
MH0822@4.asc	MH08-22d	Timberline	89	4	2.3	0.3	4.6	0.6	0.0067	0.00	0.0143	0.98
MH22_36.asc	MH08-22-36	Timberline	70	4	2.6	0.2	5.0	0.6	0.012275	1.19	0.006301	1.07
MH22_36@2.asc	MH08-22-36	Timberline	65	4	3.1	0.3	4.9	0.6	0.011358	1.26	0.007531	1.06

Filename	Sample No.	Eruptive unit	H_2O µg/g	± 2s	F µg/g	± 2s	^{12}C, cps	± $2s_{mean}$	$^{16}O^1H/^{18}O$, blank corrected	$s_{mean}/s_{Poisson}$ [$^{16}O^1H/^{18}O$]	$^{19}F/^{18}O$, blank corrected	$s_{mean}/s_{Poisson}$ [$^{19}F/^{18}O$]
MH0822chain1@0.asc	MH08-22d	Timberline	91	6	1.9	0.2	5.1	0.4	0.0147	1.15	0.0045	0.83
MH22_36@4.asc	MH08-22-36	Timberline	49	3	3.6	0.3	5.5	0.8	0.008625	1.32	0.008785	0.98
MH22_36@5.asc	MH08-22-36	Timberline	73	4	2.5	0.3	4.7	0.7	0.012817	1.24	0.006178	1.11
MH22_36@6.asc	MH08-22-36	Timberline	58	2	2.6	0.3	4.8	0.8	0.010128	0.78	0.006353	1.09
MH22_36@7.asc	MH08-22-36	Timberline	66	3	2.8	0.3	5.5	0.8	0.011539	1.08	0.006843	1.19
MH22_33.asc	MH08-22-33	Timberline	50	2	7.9	0.8	8.1	1.0	0.008765	0.89	0.019366	1.88
MH22_33@1.asc	MH08-22-33	Timberline	67	3	2.5	0.3	6.3	0.8	0.011724	1.06	0.006118	1.15
MH22_33@2.asc	MH08-22-33	Timberline	48	2	3.2	0.2	5.4	0.7	0.008489	0.95	0.007804	0.88
MH22_33@4.asc	MH08-22-33	Timberline	62	3	2.7	0.2	4.7	0.7	0.010931	0.87	0.006615	1.02
MH22_24.asc	MH08-22-24	Timberline	46	8	3.3	0.7	6.0	0.9	0.008044	1.07	0.008101	0.92
MH22_24@1.asc	MH08-22-24	Timberline	56	3	3.3	0.3	3.5	0.5	0.009811	0.92	0.008108	1.01
MH22_24@2.asc	MH08-22-24	Timberline	49	2	3.8	0.3	8.8	1.5	0.008532	0.85	0.009206	0.88
MH22_24@4.asc	MH08-22-24	Timberline	50	2	3.3	0.3	4.4	0.7	0.008753	0.86	0.00806	1.10
MH22_18@1.asc	MH08-22-18	Timberline	61	3	3.2	0.3	4.2	0.6	0.010662	1.05	0.007712	0.91
MH22_02.asc	MH08-22-02	Timberline	47	4	3.8	0.3	5.1	0.7	0.008232	1.29	0.009303	0.99
MH22_02@1.asc	MH08-22-02	Timberline	73	4	2.7	0.2	4.7	0.6	0.012916	1.04	0.006543	0.92
MH22_02@2.asc	MH08-22-02	Timberline	42	3	3.9	0.2	4.8	0.8	0.007309	1.11	0.009496	0.81
MH22_08c.asc	MH08-22-08	Timberline	89	5	2.0	0.3	6.9	1.0	0.015765	1.23	0.00476	1.15
MH22_08c@0.asc	MH08-22-08	Timberline	58	3	3.1	0.2	7.1	0.9	0.01015	1.02	0.007578	0.82
MH22_08c@1.asc	MH08-22-08	Timberline	82	4	2.1	0.3	5.4	0.9	0.014471	1.06	0.005169	1.04
MH22_08c@2.asc	MH08-22-08	Timberline	53	3	3.4	0.3	4.9	0.6	0.009281	1.17	0.008333	0.92

Filename	Sample No.	Eruptive unit	H_2O µg/g	± 2s	F µg/g	± 2s	^{12}C, cps	± $2s_{mean}$	$^{16}O^{1}H/^{18}O$, blank corrected	$s_{mean}/s_{Poisson}$ $[^{16}O^{1}H/^{18}O]$	$^{19}F/^{18}O$, blank corrected	$s_{mean}/s_{Poisson}$ $[^{19}F/^{18}O]$
MH0822chain1@0.asc	MH08-22d	Timberline	91	6	1.9	0.2	5.1	0.4	0.0147	1.15	0.0045	0.83
MH22_08c@3.asc	MH08-22-08	Timberline	83	4	2.1	0.3	4.9	0.7	0.014704	1.16	0.005042	1.17
MH22_06c@2.asc	MH08-22-06	Timberline	71	3	2.5	0.2	4.8	0.8	0.012425	0.97	0.00609	0.89
chain7.asc	MH08-22-11	Timberline	99	5	2.2	0.2	4.0	0.6	0.017435	1.26	0.005328	1.02
chain7@1.asc	MH08-22-11	Timberline	96	3	2.2	0.3	4.7	0.8	0.017017	0.78	0.005453	1.25
chain7@1.asc	MH08-22-11	Timberline	96	3	2.2	0.3	4.7	0.8	0.017017	0.78	0.005453	1.25
chain7@2.asc	MH08-22-11	Timberline	78	3	2.4	0.2	4.6	0.6	0.013787	0.91	0.005817	0.94
chain7@4.asc	MH08-22-15	Timberline	80	4	2.3	0.2	6.1	0.7	0.014169	1.09	0.005496	0.69
chain7@6.asc	MH08-22-15	Timberline	56	3	3.3	0.3	4.5	0.8	0.009814	0.84	0.007937	0.89
chain8.asc	MH08-22-28	Timberline	81	4	2.5	0.3	5.0	0.9	0.014303	1.12	0.006044	1.28
chain8@0.asc	MH08-22-28	Timberline	84	4	2.4	0.2	4.6	1.0	0.0149	1.02	0.005881	0.89
chain8@2.asc	MH08-22-28	Timberline	71	3	2.6	0.3	5.0	0.7	0.012503	0.89	0.006423	1.00
chain8@3.asc	MH08-22-29	Timberline	51	3	3.5	0.2	4.5	0.7	0.009019	1.12	0.008598	0.68
chain8@1.asc	MH08-22-29	Timberline	56	4	3.3	0.3	5.0	0.6	0.009865	1.28	0.008038	0.99
chain8@4.asc	MH08-22-29	Timberline	47	2	4.0	0.2	4.6	0.6	0.00833	0.73	0.009628	0.61
chain8@5.asc	MH08-22-28	Timberline	86	4	2.3	0.3	4.3	0.7	0.015131	1.13	0.00572	1.23
MH22_29.asc	MH08-22-32	Timberline	52	2	3.3	0.3	3.8	0.6	0.009197	0.67	0.00807	1.21
chain9.asc	MH08-23-06	Polallie	67	3	2.2	0.3	4.1	0.7	0.011857	1.03	0.005367	1.17
chain9@0.asc	MH08-23-06	Polallie	98	4	3.5	0.5	4.5	0.8	0.017269	1.18	0.008588	1.96
chain9@1.asc	MH08-23-06	Polallie	88	3	3.5	0.3	4.6	0.7	0.015534	0.78	0.008487	0.92
chain9@2.asc	MH08-23-06	Polallie	87	3	3.5	0.3	5.0	0.6	0.015396	0.79	0.008635	0.97

Filename	Sample No.	Eruptive unit	H_2O µg/g	± 2s	F µg/g	± 2s	^{12}C, cps	± $2s_{mean}$	$^{16}O^{1}H/^{18}O$, blank corrected	$s_{mean}/s_{Poisson}$ [$^{16}O^{1}H/^{18}O$]	$^{19}F/^{18}O$, blank corrected	$s_{mean}/s_{Poisson}$ [$^{19}F/^{18}O$]
MH0822chain1@0.asc	MH08-22d	Timberline	91	6	1.9	0.2	5.1	0.4	0.0147	1.15	0.0045	0.83
chain9@5.asc	MH08-23-02	Polallie	93	5	3.7	0.3	6.6	0.9	0.016338	1.30	0.00905	1.18
chain9@6.asc	MH08-23-02	Polallie	92	4	3.6	0.2	6.4	0.9	0.016308	0.98	0.008796	0.69
chain9@7.asc	MH08-23-05	Polallie	91	3	3.3	0.3	8.7	2.9	0.016116	0.95	0.008043	0.92
chain9@8.asc	MH08-23-05	Polallie	92	3	4.1	0.4	6.6	1.2	0.016217	0.92	0.010031	1.17
chain9@9.asc	MH08-23-05	Polallie	93	4	3.3	0.2	6.4	0.7	0.016347	1.04	0.007984	0.78
MH22_18@6.asc	MH08-22-18	Timberline	47	3	3.5	0.2	5.0	0.8	0.008298	0.97	0.00851	0.64
MH22_18@6.asc	MH08-22-18	Timberline	47	3	3.5	0.2	5.0	0.8	0.008298	0.97	0.00851	0.64
MH22_18@7.asc	MH08-22-18	Timberline	47	3	4.2	0.3	5.1	0.8	0.008203	1.06	0.010202	1.01
MH22_11@3.asc	MH08-22-11	Timberline	92	4	2.4	0.2	6.2	1.1	0.016157	1.01	0.005842	0.73
MH22_11@5.asc	MH08-22-11	Timberline	89	4	2.5	0.3	5.1	0.7	0.015705	1.00	0.006154	1.13
chain10@7.asc	MH08-23-13	Polallie	81	4	3.5	0.3	5.3	0.8	0.014263	1.14	0.008423	0.94
chain10@8.asc	MH08-23-13	Polallie	97	4	3.2	0.3	4.4	0.5	0.017043	1.09	0.007697	1.25
chain10@11.asc	MH08-23-14	Polallie	76	4	2.6	0.2	4.8	0.8	0.013346	1.11	0.006412	0.78
chain10@12.asc	MH08-23-14	Polallie	88	3	3.0	0.2	6.1	0.6	0.015486	0.86	0.007346	0.92
chain10@13.asc	MH08-23-17	Polallie	85	4	3.6	0.3	5.1	0.7	0.015024	1.28	0.008728	0.91
chain10@14.asc	MH08-23-17	Polallie	91	4	4.2	0.4	4.9	0.8	0.016013	1.25	0.010314	1.20
chain10@15.asc	MH08-23-17	Polallie	90	5	3.6	0.3	4.4	0.6	0.015887	1.32	0.008668	1.00
chain10@16.asc	MH08-23-15	Polallie	89	4	3.4	0.4	4.7	0.6	0.015719	1.12	0.008195	1.34
chain10@17.asc	MH08-23-15	Polallie	85	3	3.3	0.2	4.3	0.7	0.014906	1.03	0.008022	0.70
chain10@18.asc	MH08-23-15	Polallie	98	3	3.3	0.3	4.3	0.6	0.017358	0.90	0.008065	1.09

Filename	Sample No.	Eruptive unit	H_2O µg/g	± 2s	F µg/g	± 2s	^{12}C, cps	± $2s_{mean}$	$^{16}O^1H/^{18}O$, blank corrected	$s_{mean}/s_{Poisson}$ [$^{16}O^1H/^{18}O$]	$^{19}F/^{18}O$, blank corrected	$s_{mean}/s_{Poisson}$ [$^{19}F/^{18}O$]
MH0822chain1@0.asc	MH08-22d	Timberline	91	6	1.9	0.2	5.1	0.4	0.0147	1.15	0.0045	0.83
chain10@19.asc	MH08-23-16	Polallie	88	3	3.4	0.2	5.4	0.8	0.015613	0.90	0.008362	0.72
chain10@20.asc	MH08-23-16	Polallie	93	4	3.5	0.2	5.2	1.0	0.016383	1.09	0.008518	0.84
chain10@21.asc	MH08-23-16	Polallie	92	6	3.2	0.2	5.1	0.8	0.0163	1.63	0.007719	0.73
chain10@23.asc	MH08-23-16	Polallie	0	1	19.6	0.5	4.6	0.8	-2.28E-05	1.28	0.047756	0.80
MH20_03.asc	MH08-20-03	Old Maid	9	1	1.5	0.1	4.4	0.6	0.001495	1.05	0.00373	0.74
MH20_03@1.asc	MH08-20-03	Old Maid	7	1	1.8	0.2	3.6	0.8	0.001198	0.90	0.004323	0.97
MH20_03@2.asc	MH08-20-03	Old Maid	9	1	2.4	0.3	3.8	0.8	0.001526	1.15	0.005913	1.43
MH20_03@3.asc	MH08-20-03	Old Maid	7	1	1.8	0.2	4.6	0.5	0.001142	0.90	0.004479	1.00
MH20_09.asc	MH08-20-09	Old Maid	15	2	3.8	0.3	5.3	0.6	0.002528	1.24	0.009382	0.96
MH20_09@1.asc	MH08-20-09	Old Maid	3	1	2.8	0.2	4.7	0.6	0.000508	0.79	0.006752	0.75
MH20_09@2.asc	MH08-20-09	Old Maid	11	1	4.3	0.5	5.0	0.7	0.001937	0.89	0.010535	1.66
MH20_09@4.asc	MH08-20-09	Old Maid	13	2	1.6	0.2	4.5	0.7	0.002252	1.09	0.003836	1.01
MH20_09@5.asc	MH08-20-09	Old Maid	4	1	3.0	0.3	5.3	0.6	0.000582	1.05	0.007271	1.03
MH20_09c.asc	MH08-20-09	Old Maid	9	1	2.7	0.2	4.3	0.6	0.001589	1.08	0.006656	0.92
MH20_09c@0.asc	MH08-20-09	Old Maid	10	2	3.0	0.2	5.1	0.4	0.001752	1.70	0.007339	0.75
MH20_09c@1.asc	MH08-20-09	Old Maid	16	2	3.7	0.3	4.6	0.8	0.002748	1.43	0.009074	1.25
MH20_09c@2.asc	MH08-20-09	Old Maid	16	1	4.2	0.2	4.9	0.9	0.002762	0.94	0.010241	0.77
MH20_09c@6.asc	MH08-20-09	Old Maid	17	2	3.2	0.3	5.1	0.7	0.002845	1.26	0.007792	1.05
MH20_09c@7.asc	MH08-20-09	Old Maid	12	2	3.3	0.2	4.6	0.4	0.002046	1.43	0.008116	0.74
MH20_09c@8.asc	MH08-20-09	Old Maid	15	2	3.6	0.3	5.5	0.7	0.002541	1.35	0.008756	1.19

Filename	Sample No.	Eruptive unit	H_2O µg/g	± 2s	F µg/g	± 2s	^{12}C, cps	± $2s_{mean}$	$^{16}O^{1}H/^{18}O$, blank corrected	$s_{mean}/s_{Poisson}$ [$^{16}O^{1}H/^{18}O$]	$^{19}F/^{18}O$, blank corrected	$s_{mean}/s_{Poisson}$ [$^{19}F/^{18}O$]
MH0822chain1@0.asc	MH08-22d	Timberline	91	6	1.9	0.2	5.1	0.4	0.0147	1.15	0.0045	0.83
MH20_09c@9.asc	MH08-20-09	Old Maid	13	2	2.5	0.3	4.0	0.7	0.002295	1.12	0.006186	1.24
MH20_09c@10.asc	MH08-20-09	Old Maid	10	1	2.5	0.3	5.1	0.7	0.001616	1.02	0.006001	1.13
MH22_08c2.asc	MH08-22-08	Timberline	65	5	2.8	0.3	3.9	0.7	0.011467	1.53	0.006811	1.06
MH22_08c2@0.asc	MH08-22-08	Timberline	89	4	2.2	0.2	5.6	0.8	0.015775	1.08	0.005269	0.87
MH22_08c2@1.asc	MH08-22-08	Timberline	91	3	2.0	0.2	5.8	0.9	0.015971	0.99	0.004871	0.82
MH22_08c2@2.asc	MH08-22-08	Timberline	94	3	2.1	0.2	4.6	0.5	0.016559	0.94	0.005095	0.79
MH22_08c2@4.asc	MH08-22-08	Timberline	90	3	2.0	0.2	4.8	0.8	0.01581	0.85	0.00488	1.14
MH22_08c2@5.asc	MH08-22-08	Timberline	85	3	2.1	0.2	4.2	0.5	0.015073	0.83	0.005202	1.10
MH22_11c.asc	MH08-22-11	Timberline	103	4	2.2	0.2	4.7	0.7	0.018145	1.17	0.005328	0.98
MH22_11c@0.asc	MH08-22-11	Timberline	87	4	2.3	0.3	4.8	0.6	0.015377	1.12	0.005689	1.12
MH22_11c@1.asc	MH08-22-11	Timberline	94	4	2.3	0.2	5.2	0.6	0.01652	1.23	0.005603	0.75
MH22_11c@2.asc	MH08-22-11	Timberline	100	5	2.1	0.2	4.0	0.6	0.017658	1.35	0.005119	0.84
MH22_11c@3.asc	MH08-22-11	Timberline	100	4	2.1	0.2	4.8	0.7	0.017648	1.14	0.005148	1.02
MH22_11c@4.asc	MH08-22-11	Timberline	103	4	2.3	0.2	4.0	0.7	0.018137	1.02	0.005519	0.86
MH22_11c@5.asc	MH08-22-11	Timberline	103	5	2.3	0.2	4.0	0.6	0.018221	1.35	0.005518	0.85
MH23_06c.asc	MH08-23-06	Polallie	82	9	2.5	0.2	4.1	0.8	0.014421	2.80	0.005987	1.01
MH23_06c@0.asc	MH08-23-06	Polallie	79	6	3.1	0.3	4.3	0.6	0.014009	1.99	0.007643	1.02
MH23_06c@1.asc	MH08-23-06	Polallie	87	8	3.1	0.3	3.5	0.6	0.015354	2.28	0.007452	1.10
MH23_06c@3.asc	MH08-23-06	Polallie	90	7	3.2	0.2	3.8	0.8	0.015808	2.22	0.007828	0.95
MH23_06c@4.asc	MH08-23-06	Polallie	78	7	2.8	0.2	4.7	0.8	0.013715	2.14	0.006922	0.95

Filename	Sample No.	Eruptive unit	H_2O µg/g	± 2s	F µg/g	± 2s	^{12}C, cps	± $2s_{mean}$	$^{16}O^1H/^{18}O$, blank corrected	$s_{mean}/s_{Poisson}$ [$^{16}O^1H/^{18}O$]	$^{19}F/^{18}O$, blank corrected	$s_{mean}/s_{Poisson}$ [$^{19}F/^{18}O$]
MH0822chain1@0.asc	MH08-22d	Timberline	91	6	1.9	0.2	5.1	0.4	0.0147	1.15	0.0045	0.83
MH23_06c@5.asc	MH08-23-06	Polallie	69	5	2.9	0.3	4.2	0.7	0.012113	1.65	0.006965	1.31
chain12@33.asc	MH08-20-04	Old Maid	30	3	0.0	0.1	4.5	0.5	0.005287	1.56	2.68E-05	0.97
chain12@35.asc	MH08-20-04	Old Maid	17	2	2.1	0.2	4.1	0.6	0.002969	1.34	0.005016	0.84
chain12@36.asc	MH08-20-04	Old Maid	35	3	2.4	0.2	4.3	0.7	0.006073	1.33	0.005821	1.01
chain12@37.asc	MH08-20-04	Old Maid	43	4	2.6	0.4	4.3	0.8	0.007489	1.61	0.006399	1.86
chain12@38.asc	MH08-20-04	Old Maid	37	3	3.6	0.3	4.0	0.7	0.006558	1.46	0.008699	1.15
chain12@39.asc	MH08-20-04	Old Maid	16	2	3.4	0.2	4.3	0.8	0.002674	1.28	0.008257	0.85
chain12@40.asc	MH08-20-04	Old Maid	7	1	2.8	0.2	3.7	0.7	0.001096	1.25	0.00694	1.02
chain12@41.asc	MH08-20-04	Old Maid	9	1	2.3	0.2	3.2	0.6	0.001557	1.13	0.005613	1.16
chain12@42.asc	MH08-20-04	Old Maid	1	1	2.7	0.2	3.5	0.5	8.77E-05	0.96	0.006523	0.91
chain12@43.asc	MH08-20-04	Old Maid	3	1	2.9	0.2	3.4	0.6	0.000385	1.27	0.007042	0.84
chain12@44.asc	MH08-20-04	Old Maid	4	1	3.1	0.2	4.1	0.6	0.000653	0.92	0.007461	0.84
chain12@45.asc	MH08-20-04	Old Maid	15	2	2.5	0.2	3.9	0.7	0.002555	1.03	0.006176	0.85
chain12@46.asc	MH08-20-04	Old Maid	36	3	2.2	0.2	3.9	0.6	0.006228	1.33	0.005261	1.08
chain12@48.asc	MH08-20-04	Old Maid	4	1	2.9	0.2	3.4	0.6	0.000605	1.28	0.007171	0.90

Appendix C: Calibration curves and standards used

H_2O 2018	
Type	York fit
Intercept	-0.54339
Slope	5633.136
MSWD	0.091881
p-value	0.964581

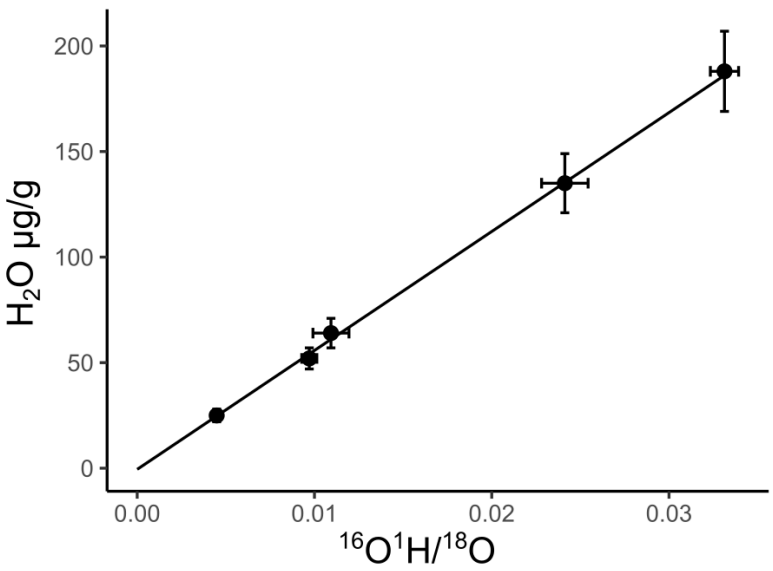

F 2018	
Type	OLS
Intercept	0
Slope	410.4
R^2	0.9853

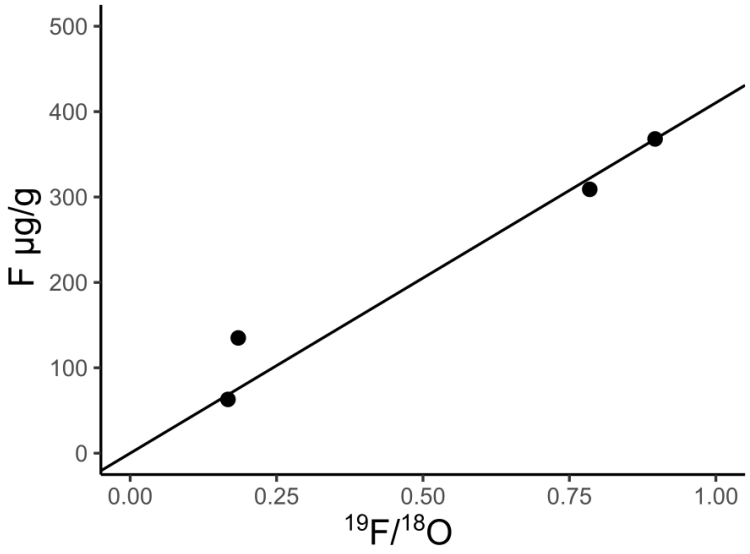

H_2O 2016	
Type	York fit
Intercept	-0.90016
Slope	6123.436
MSWD	0.43564
p-value	0.78296

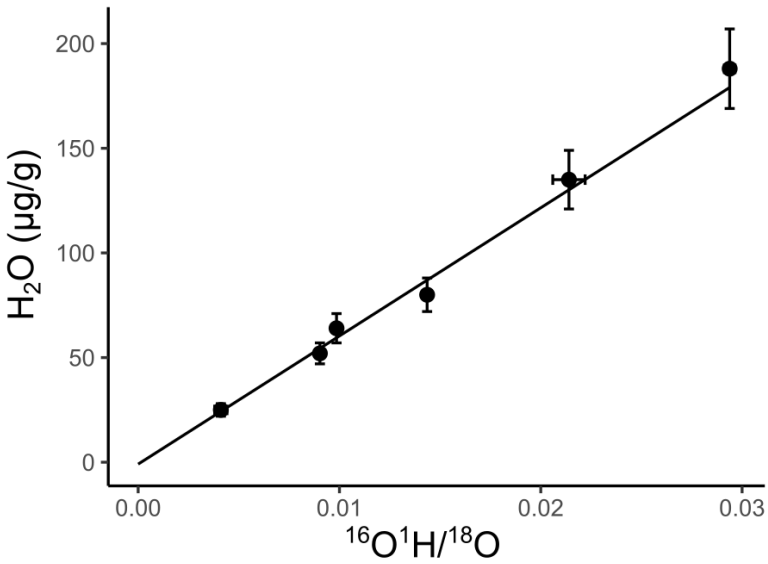

F 2016	
Type	OLS
Intercept	0
Slope	412.8
R^2	0.9997

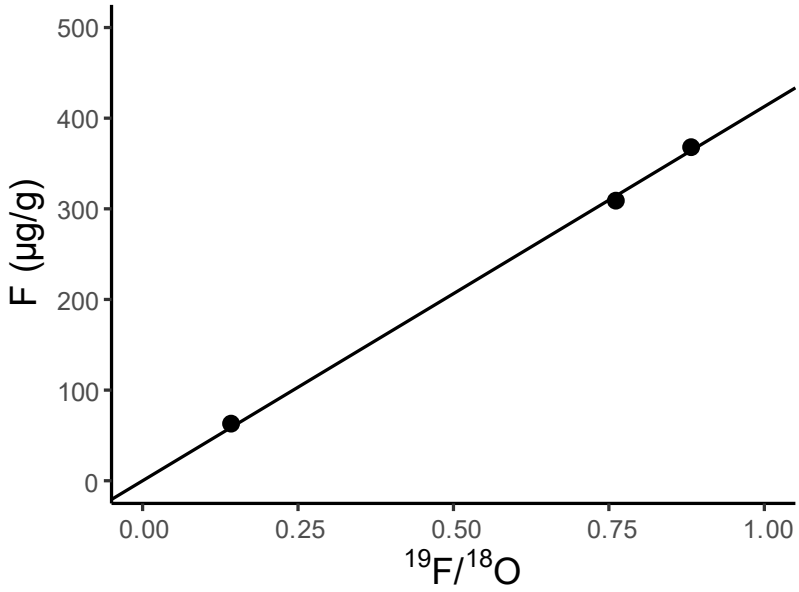

Standards used:

Name	Type	H2O	2σ	F
GRR1017	Blank (olivine)	0		0
GRR145	Blank (plag)	0		0
BCR-2G	Glass			368
KL2-G	Glass			135
BHVO-2G	Glass			309
ML3B-G	Glass			63
GRR2651	Plag	0.7	2	
GRR1604	Plag	25	3	
GRR580	Plag	64	7	
GRR25	Plag	80	8	
GRR1389	Plag	188	19	
GRR1679	Plag	52	5	
GRR1280	Plag	135	14	

Plagioclase standards from Mosenfelder et al. 2015, fluorine glass standards from Guggino and Hervig 2011.

Appendix D: Major element analyses

Sample	SiO_2	TiO_2	Al_2O_3	Cr_2O_3	CaO	MgO	MnO	FeO	K_2O	Na_2O	Total	An	Ab	Or
MH08_20a														
	55.3	0.0	29.9	0.0	11.4	0.0	0.0	0.3	0.2	5.0	102.2	55.1	43.9	1.0
	52.7	0.0	32.2	0.0	13.7	0.0	0.0	0.3	0.1	3.8	102.8	66.4	33.1	0.5
	56.5	0.0	29.7	0.0	10.8	0.0	0.0	0.3	0.2	5.3	102.8	52.4	46.6	0.9
MH08_20c														
	58.2	0.0	27.4	0.0	8.9	0.0	0.0	0.3	0.2	6.4	101.5	43.0	55.6	1.4
	59.4	0.0	27.2	0.0	8.7	0.0	0.0	0.4	0.2	6.6	102.6	41.7	56.9	1.4
	57.6	0.0	28.5	0.0	9.8	0.0	0.0	0.3	0.2	5.9	102.4	47.2	51.6	1.2
	57.2	0.0	28.6	0.0	10.1	0.0	0.0	0.3	0.2	5.7	102.1	48.8	50.0	1.2
	58.0	0.0	28.3	0.0	9.8	0.0	0.0	0.3	0.2	6.0	102.7	46.7	51.9	1.3
	59.0	0.0	27.7	0.0	9.0	0.0	0.0	0.3	0.3	6.3	102.6	43.4	55.1	1.5
	59.5	0.0	27.7	0.0	8.7	0.0	0.0	0.4	0.3	6.4	103.0	42.5	56.0	1.5
	57.9	0.0	28.0	0.0	9.4	0.0	0.0	0.4	0.2	6.1	102.0	45.4	53.3	1.3
	56.2	0.0	28.8	0.0	10.3	0.0	0.0	0.3	0.2	5.5	101.4	50.1	48.6	1.3
	55.4	0.0	29.1	0.0	10.7	0.0	0.0	0.3	0.2	5.2	101.0	52.5	46.6	0.9

Sample	SiO_2	TiO_2	Al_2O_3	Cr_2O_3	CaO	MgO	MnO	FeO	K_2O	Na_2O	Total	An	Ab	Or
MH08_20d														
	57.4	0.0	28.0	0.0	9.6	0.0	0.0	0.3	0.2	5.9	101.5	46.7	52.1	1.2
	57.7	0.0	28.4	0.0	9.6	0.0	0.0	0.3	0.2	5.9	102.2	46.7	52.0	1.3
	59.9	0.0	26.2	0.0	7.4	0.0	0.0	0.3	0.3	7.0	101.1	36.4	61.8	1.8
	57.3	0.0	28.6	0.0	9.8	0.0	0.0	0.3	0.2	5.9	102.2	47.3	51.5	1.2
	58.7	0.0	27.5	0.0	8.7	0.0	0.0	0.3	0.2	6.4	102.0	42.3	56.3	1.4
	56.1	0.0	29.1	0.0	10.6	0.0	0.0	0.3	0.2	5.5	101.9	51.0	48.1	0.9
MH08_22a														
	58.0	0.0	28.5	0.0	9.7	0.0	0.0	0.3	0.2	6.0	102.7	46.6	52.1	1.3
	57.5	0.0	28.8	0.0	10.0	0.0	0.0	0.3	0.2	5.8	102.6	48.4	50.3	1.3
	54.9	0.0	30.4	0.0	11.9	0.0	0.0	0.3	0.2	4.8	102.6	57.0	42.1	0.9
	53.4	0.0	31.5	0.0	13.0	0.0	0.0	0.3	0.1	4.1	102.5	63.3	36.2	0.5
	56.1	0.0	29.3	0.0	10.8	0.0	0.0	0.2	0.2	5.6	102.3	51.2	47.9	0.9
	52.9	0.0	31.8	0.0	13.6	0.0	0.0	0.4	0.1	4.0	102.9	64.9	34.6	0.6
	52.2	0.0	32.0	0.0	13.7	0.0	0.0	0.4	0.1	3.7	102.1	67.1	32.4	0.5
	51.7	0.1	32.1	0.0	13.8	0.0	0.0	0.4	0.1	3.7	101.8	67.2	32.2	0.6
	51.5	0.0	31.1	0.0	13.4	0.0	0.0	0.3	0.1	3.8	100.4	65.6	33.7	0.7

Sample	SiO_2	TiO_2	Al_2O_3	Cr_2O_3	CaO	MgO	MnO	FeO	K_2O	Na_2O	Total	An	Ab	Or
	62.8	0.1	22.7	0.0	5.9	0.1	0.0	0.7	1.3	5.8	99.4	32.8	58.4	8.8
	58.4	0.0	27.7	0.0	8.9	0.0	0.0	0.3	0.2	6.3	101.9	43.3	55.3	1.4
	57.2	0.0	28.4	0.0	9.9	0.0	0.0	0.3	0.2	5.8	101.8	47.7	51.1	1.1
	57.2	0.0	26.7	0.0	8.3	0.0	0.0	0.3	0.3	9.5	102.3	32.0	66.8	1.2
	57.6	0.0	27.4	0.0	8.9	0.0	0.0	0.3	0.3	6.3	101.0	43.2	55.4	1.5
*mixed w/ MI	75.1	0.2	14.1	0.0	1.3	0.3	0.0	1.6	2.7	1.7	97.0	17.1	40.1	42.8
*mixed w/ MI	73.5	0.2	14.2	0.0	1.3	0.3	0.1	1.8	3.0	3.1	97.4	12.0	54.0	34.0
MH08_22b														
	56.5	0.0	28.6	0.0	9.9	0.0	0.0	0.4	0.2	5.7	101.4	48.4	50.3	1.3
	57.6	0.0	26.4	0.0	8.2	0.0	0.0	0.4	0.3	6.5	99.4	40.3	57.9	1.7
	56.2	0.0	27.5	0.0	9.4	0.0	0.0	0.4	0.2	6.0	99.7	46.1	52.6	1.4
	56.8	0.0	27.8	0.0	9.4	0.0	0.0	0.4	0.3	5.8	100.5	46.4	52.1	1.5
	53.7	0.0	28.9	0.0	10.9	0.0	0.0	0.3	0.2	5.1	99.3	53.7	45.4	1.0
	55.8	0.0	27.7	0.0	9.7	0.0	0.0	0.3	0.2	5.8	99.6	47.6	51.1	1.3
	55.9	0.0	27.3	0.0	9.3	0.0	0.0	0.4	0.2	6.0	99.1	45.4	53.2	1.4
	58.6	0.0	27.0	0.0	8.6	0.0	0.0	0.3	0.3	6.5	101.4	41.7	56.6	1.7
	59.1	0.0	27.6	0.0	8.9	0.0	0.0	0.4	0.3	6.5	102.8	42.6	55.8	1.6

Sample	SiO_2	TiO_2	Al_2O_3	Cr_2O_3	CaO	MgO	MnO	FeO	K_2O	Na_2O	Total	An	Ab	Or
MH08_22c														
	56.7	0.0	29.1	0.0	10.7	0.0	0.0	0.2	0.2	5.4	102.3	51.8	47.1	1.0
	57.3	0.0	28.8	0.0	10.2	0.0	0.0	0.2	0.2	5.6	102.4	49.5	49.4	1.2
	59.6	0.0	26.7	0.0	8.1	0.0	0.0	0.3	0.3	6.9	101.9	38.8	59.5	1.7
	52.3	0.0	31.0	0.0	13.0	0.0	0.0	0.3	0.1	3.9	100.7	64.4	35.1	0.6
	55.3	0.0	28.6	0.0	10.4	0.0	0.0	0.3	0.2	5.7	100.5	49.5	49.4	1.1
	55.2	0.0	28.7	0.0	10.1	0.0	0.0	0.3	0.2	5.7	100.3	49.3	49.7	1.0
	51.6	0.0	30.3	0.0	12.6	0.0	0.0	0.3	0.1	4.3	99.2	61.5	37.8	0.7
	54.1	0.0	29.7	0.0	11.7	0.0	0.0	0.2	0.2	4.9	100.8	56.2	42.9	0.9
	56.4	0.0	28.5	0.0	10.2	0.0	0.0	0.3	0.2	5.7	101.4	49.1	49.8	1.1
	56.3	0.0	28.8	0.0	10.4	0.0	0.0	0.2	0.2	5.6	101.5	50.0	48.7	1.3
	60.0	0.0	27.3	0.0	8.4	0.0	0.1	0.3	0.3	6.7	103.0	40.3	58.0	1.7
	53.0	0.0	30.1	0.0	12.0	0.0	0.0	0.3	0.1	4.7	100.4	58.2	41.1	0.7
	56.6	0.0	28.2	0.0	9.8	0.0	0.0	0.3	0.2	5.8	100.8	47.9	51.0	1.1
	55.3	0.0	29.5	0.0	11.2	0.0	0.0	0.2	0.2	5.2	101.6	54.1	45.0	1.0
	56.5	0.0	28.4	0.0	9.9	0.0	0.0	0.2	0.2	5.8	101.0	48.0	50.8	1.2
	55.7	0.0	29.0	0.0	10.6	0.0	0.0	0.2	0.2	5.5	101.2	50.9	47.9	1.1

Sample	SiO_2	TiO_2	Al_2O_3	Cr_2O_3	CaO	MgO	MnO	FeO	K_2O	Na_2O	Total	An	Ab	Or
	57.6	0.0	27.6	0.0	9.1	0.0	0.0	0.3	0.3	6.3	101.2	43.7	54.9	1.5
	57.5	0.0	27.5	0.0	9.2	0.0	0.0	0.3	0.2	6.3	101.1	44.2	54.4	1.4
	60.4	0.0	26.2	0.0	7.5	0.0	0.0	0.2	0.3	7.1	101.8	36.3	61.8	1.8
MH08_22d														
	53.7	0.0	30.7	0.0	12.5	0.0	0.0	0.4	0.1	4.6	102.2	59.5	39.8	0.7
	59.1	0.0	27.8	0.0	8.9	0.0	0.0	0.3	0.2	6.5	102.9	42.5	56.1	1.4
	58.3	0.0	26.9	0.0	8.3	0.0	0.0	0.2	0.3	6.7	100.8	40.0	58.4	1.6
	58.2	0.0	27.7	0.0	9.1	0.0	0.0	0.3	0.2	6.4	102.0	43.3	55.3	1.3
	58.1	0.0	27.7	0.0	9.2	0.0	0.0	0.2	0.3	6.5	102.0	43.4	55.1	1.5
	57.8	0.0	27.2	0.0	8.8	0.0	0.0	0.2	0.2	6.5	100.8	42.1	56.5	1.3
	52.5	0.0	30.7	0.0	12.6	0.0	0.0	0.3	0.1	4.4	100.6	61.1	38.2	0.7
	55.0	0.0	29.0	0.0	11.0	0.0	0.0	0.3	0.2	5.5	101.0	52.1	46.9	1.0
MH08_23a														
	58.7	0.0	27.3	0.0	8.9	0.0	0.0	0.4	0.2	6.5	102.2	42.6	56.2	1.2
	58.6	0.0	27.5	0.0	9.1	0.0	0.0	0.4	0.2	6.4	102.2	43.6	55.3	1.2
	58.7	0.0	27.7	0.0	9.0	0.0	0.0	0.4	0.2	6.4	102.4	43.2	55.6	1.2
	57.9	0.0	28.3	0.0	9.7	0.0	0.0	0.3	0.2	6.1	102.5	46.2	52.8	1.0

Sample	SiO_2	TiO_2	Al_2O_3	Cr_2O_3	CaO	MgO	MnO	FeO	K_2O	Na_2O	Total	An	Ab	Or
	57.5	0.0	28.2	0.0	9.9	0.0	0.0	0.4	0.2	5.9	102.2	47.7	51.2	1.1
	58.2	0.0	27.6	0.0	9.2	0.0	0.0	0.3	0.2	6.2	101.8	44.3	54.4	1.3
MH08_23b														
	57.3	0.0	28.3	0.0	9.7	0.0	0.0	0.3	0.2	5.9	101.8	47.2	51.7	1.1
	57.6	0.0	27.4	0.0	9.1	0.0	0.0	0.3	0.2	6.5	101.2	43.2	55.6	1.2
	59.2	0.0	26.6	0.0	7.9	0.0	0.0	0.3	0.3	7.0	101.3	37.9	60.6	1.5
	58.3	0.0	27.1	0.0	8.6	0.0	0.0	0.3	0.2	6.6	101.1	41.4	57.4	1.2
	56.5	0.0	28.4	0.0	10.4	0.0	0.0	0.3	0.2	5.6	101.4	49.9	49.0	1.1
	57.8	0.0	27.6	0.0	9.2	0.0	0.0	0.4	0.2	6.1	101.4	44.7	54.0	1.2
	57.7	0.0	28.2	0.0	9.6	0.0	0.0	0.3	0.2	6.0	102.2	46.2	52.6	1.2
	57.4	0.0	28.4	0.0	9.8	0.0	0.0	0.3	0.2	5.8	102.0	47.6	51.3	1.0
	59.1	0.0	27.3	0.0	8.8	0.0	0.0	0.4	0.2	6.5	102.3	42.4	56.3	1.3
	59.2	0.0	26.9	0.0	8.5	0.0	0.0	0.3	0.2	6.5	101.6	41.3	57.3	1.4
	58.8	0.0	27.6	0.0	8.9	0.0	0.0	0.3	0.2	6.3	102.3	43.2	55.5	1.3
	57.3	0.0	28.4	0.0	9.9	0.0	0.0	0.4	0.2	5.9	102.1	47.7	51.3	1.1
	57.1	0.0	28.6	0.0	10.1	0.0	0.0	0.3	0.2	5.9	102.1	48.1	50.9	0.9
	57.6	0.0	28.1	0.0	9.7	0.0	0.0	0.3	0.2	6.0	102.0	46.5	52.4	1.1

Sample	SiO_2	TiO_2	Al_2O_3	Cr_2O_3	CaO	MgO	MnO	FeO	K_2O	Na_2O	Total	An	Ab	Or
	55.9	0.1	29.3	0.0	10.9	0.0	0.0	0.3	0.1	5.3	102.0	52.8	46.4	0.8
	58.7	0.1	27.3	0.0	8.8	0.0	0.0	0.4	0.2	6.5	101.9	42.3	56.3	1.3
MH08_23c														
	57.8	0.0	27.6	0.0	9.3	0.0	0.0	0.4	0.2	6.3	101.6	44.3	54.4	1.2
	58.6	0.0	26.9	0.0	8.4	0.0	0.0	0.3	0.2	6.8	101.2	40.3	58.4	1.3
	57.7	0.0	27.8	0.0	9.3	0.0	0.0	0.3	0.2	6.1	101.5	45.2	53.6	1.2
	57.7	0.0	27.5	0.0	9.5	0.0	0.0	0.2	0.2	6.2	101.3	45.2	53.6	1.2
MH08_23d														
	57.1	0.0	27.2	0.0	9.3	0.0	0.0	0.3	0.2	6.1	100.3	45.4	53.5	1.1
	56.4	0.0	28.4	0.0	10.2	0.0	0.0	0.3	0.2	5.8	101.3	49.0	50.1	0.9
	56.7	0.0	28.4	0.0	10.2	0.0	0.0	0.3	0.2	5.7	101.5	49.1	49.8	1.1
	56.9	0.0	28.5	0.0	10.3	0.0	0.0	0.3	0.2	5.7	101.9	49.6	49.4	1.0
	56.7	0.0	29.0	0.0	10.8	0.0	0.0	0.3	0.2	5.4	102.5	51.9	47.2	0.9
	58.0	0.0	28.2	0.0	9.7	0.0	0.0	0.4	0.2	6.0	102.6	46.4	52.3	1.2
	55.0	0.0	28.2	0.0	10.7	0.0	0.0	0.3	0.2	5.3	99.7	52.2	46.9	0.9
	56.2	0.0	27.3	0.0	9.6	0.0	0.0	0.4	0.2	6.0	99.7	46.5	52.4	1.2
	57.2	0.0	26.9	0.0	9.2	0.0	0.0	0.4	0.2	6.3	100.2	44.1	54.8	1.2

MH08-20-04(4)

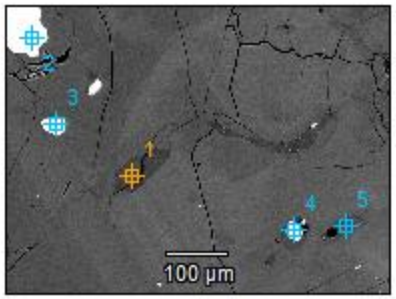

Image Name:	MH08-20-04(4)
Image Resolution:	2048 by 1536
Image Pixel Size:	0.31 µm
Acc. Voltage:	15.0 kV
Magnification:	180

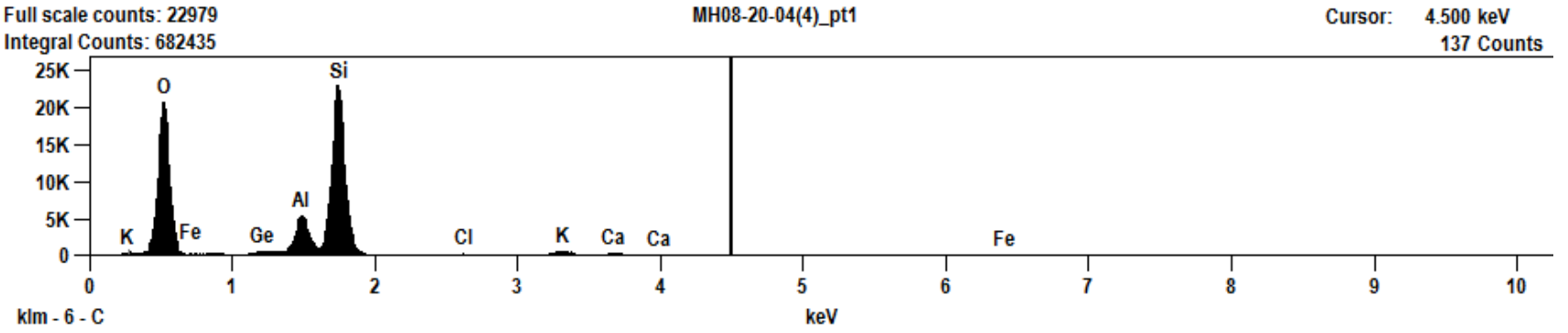
Full scale counts: 22979
Integral Counts: 682435
MH08-20-04(4)_pt1
Cursor: 4.500 keV
137 Counts
25K
20K
15K
10K
5K
0
O
Si
Al
K
Fe
Ge
Cl
K
Ca
Ca
Fe
0
1
2
3
4
5
6
7
8
9
10
klm - 6 - C
keV

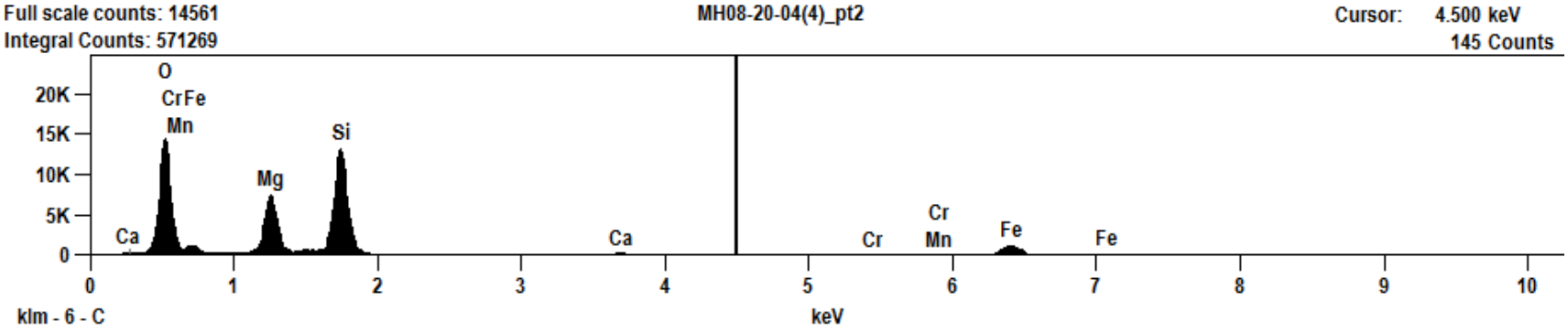
Full scale counts: 14561
Integral Counts: 571269
MH08-20-04(4)_pt2
Cursor: 4.500 keV
145 Counts
20K
15K
10K
5K
0
O
Cr Fe
Mn
Si
Mg
Ca
Ca
Cr
Cr
Mn
Fe
Fe
0
1
2
3
4
5
6
7
8
9
10
klm - 6 - C
keV

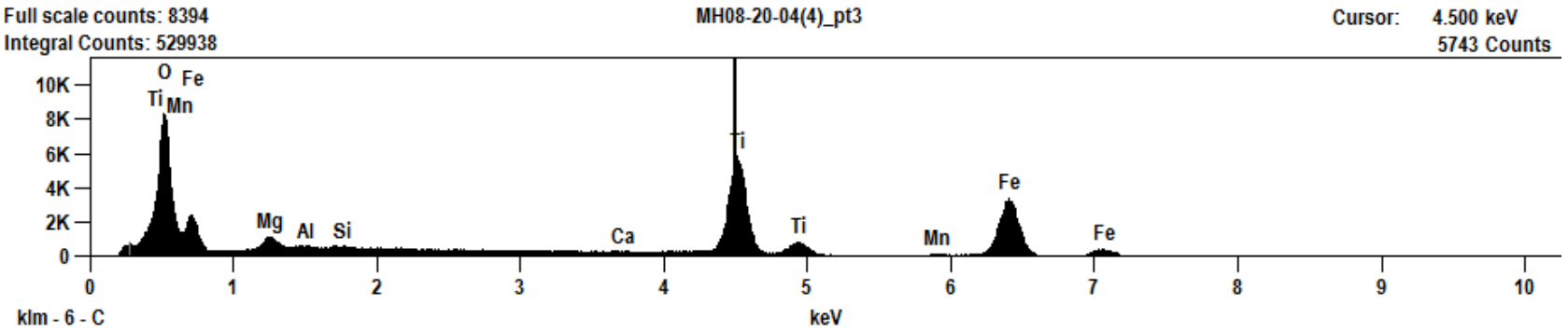
Full scale counts: 8394
Integral Counts: 529938
MH08-20-04(4)_pt3
Cursor: 4.500 keV
5743 Counts
10K
8K
6K
4K
2K
0
O
Fe
Ti
Mn
Mg
Al
Si
Ca
Ti
Ti
Mn
Fe
Fe
0 1 2 3 4 5 6 7 8 9 10
klm - 6 - C
keV

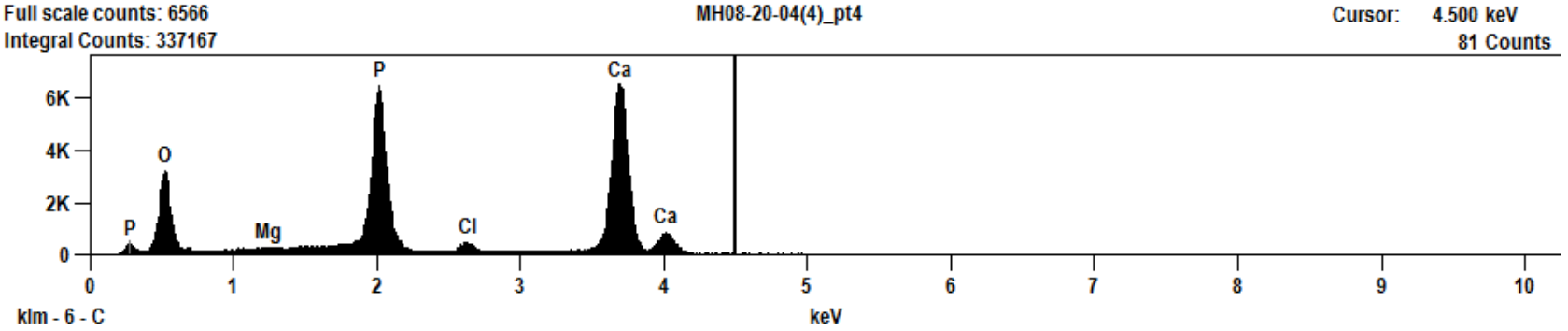
Full scale counts: 6566
Integral Counts: 337167
MH08-20-04(4)_pt4
Cursor: 4.500 keV
81 Counts
6K
4K
2K
0
P
O
Mg
P
Cl
Ca
Ca
0 1 2 3 4 5 6 7 8 9 10
klm - 6 - C
keV

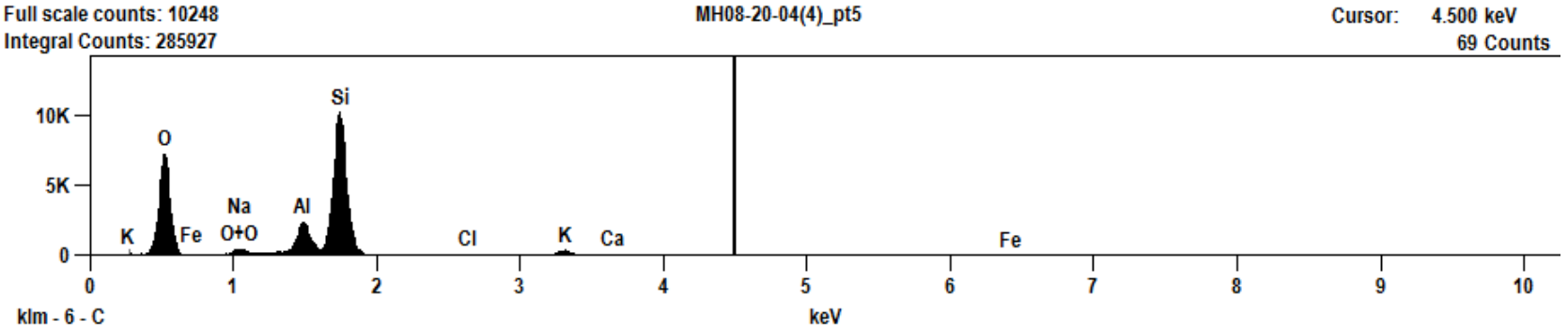
Full scale counts: 10248
Integral Counts: 285927
MH08-20-04(4)_pt5
Cursor: 4.500 keV
69 Counts
10K
5K
0
Si
O
Na
Al
K
Fe
O+O
Cl
K
Ca
Fe
0 1 2 3 4 5 6 7 8 9 10
klm - 6 - C
keV

Weight %

	C	O	Na	Mg	Al	Si	P	Cl	K	Ca	Ti	Cr	Mn	Fe	Ge
MH08-20-04(4)_pt1		50.31S			6.72	37.24		0.22	2.01	1.02				0.92	1.57
MH08-20-04(4)_pt2		44.16S		12.69		24.46				0.74		0.10	0.54	17.31	
MH08-20-04(4)_pt3		34.87S		1.35	0.13	0.14				0.24	27.25		0.53	35.50	
MH08-20-04(4)_pt4	4.72	45.97S		0.09			15.84	1.12		32.26					
MH08-20-04(4)_pt5		49.82S	2.01		6.68	36.79		0.32	2.59	0.89				0.90	

Weight % Error (+/- 1 Sigma)

	C	O	Na	Mg	Al	Si	P	Cl	K	Ca	Ti	Cr	Mn	Fe	Ge
MH08-20-04(4)_pt1		±0.18			±0.08	±0.13		±0.02	±0.06	±0.06				±0.11	±0.08
MH08-20-04(4)_pt2		±1.67		±0.08		±0.09				±0.05		±0.04	±0.06	±0.24	
MH08-20-04(4)_pt3		±0.43		±0.04	±0.02	±0.02				±0.05	±0.16		±0.06	±0.30	
MH08-20-04(4)_pt4	±0.12	±0.38		±0.02			±0.10	±0.05		±0.18					
MH08-20-04(4)_pt5		±0.24	±0.08		±0.10	±0.17		±0.06	±0.09	±0.08				±0.10	

Compound %

	CO2	(null)	Na2O	MgO	Al2O3	SiO2	P2O5	Cl	K2O	CaO	TiO2	Cr2O3	MnO	Fe2O3	GeO2
MH08-20-04(4)_pt1		0.00			12.70	79.66		0.22	2.42	1.43				1.32	2.26
MH08-20-04(4)_pt2		0.00		21.05		52.33				1.03		0.14	0.70	24.75	
MH08-20-04(4)_pt3		0.00		2.23	0.25	0.30				0.34	45.45		0.68	50.76	
MH08-20-04(4)_pt4	17.29	0.00		0.14			36.30	1.12		45.14					
MH08-20-04(4)_pt5		0.00	2.71		12.62	78.70		0.32	3.12	1.24				1.29	